Cancer Letters 604 (2024) 217221

Contents lists available at ScienceDirect

Cancer Letters

journal homepage: www.elsevier.com/locate/canlet

Original Articles

Increasing membrane polyunsaturated fatty acids sensitizes non-small cell lung cancer to anti-PD-1/PD-L1 immunotherapy☆

Sofia La Vecchia [a,1], Simona Fontana [a,b], Iris Chiara Salaroglio [a,b], Dario Pasquale Anobile [a,2], Sabrina Digiovanni [a,b], Muhlis Akman [a], Niloufar Jafari [a,b], Martina Godel [a,b], Costanzo Costamagna [a,b], Cyril Corbet [c], Joanna Kopecka [a,b,3], Chiara Riganti [a,b,*,3]

[a] Department of Oncology University of Torino, Italy
[b] Molecular Biotechnology Center "Guido Tarone", University of Torino, Italy
[c] Pole of Pharmacology and Therapeutics (FATH), Institut de Recherche Expérimentale et Clinique (IREC), UCLouvain, Brussels, Belgium

ARTICLE INFO

Keywords:
Non-small cell lung cancer
Immune checkpoints inhibitors
Phospholipidome
Letrozole
Docosahexaenoic acid

ABSTRACT

Immune checkpoints inhibitors (ICIs) as anti-PD-1/anti-PD-L1 have been approved as first-line treatment in patients with non-small cell lung cancer (NSCLC), but only 25 % of patients achieve durable response. We previously unveiled that estrogen receptor α transcriptionally up-regulates PD-L1 and aromatase inhibitors such as letrozole increase the efficacy of pembrolizumab. Here we investigated if letrozole may have additional immune-sensitizing mechanisms. We found that higher the level of PD-L1 in NSCLC, higher the activation of SREBP1c that transcriptionally increases fatty acid synthase and stearoyl-CoA desaturase enzymes, increasing the amount of polyunsaturated fatty acids (PUFAs). Letrozole further up-regulated SREBP1c-mediated transcription of lipogenic genes, and increased the amount of PUFAs, thereby leading to greater membrane fluidity and reduced binding between PD-L1 and PD-1. The same effects were observed upon supplementation with ω3-PUFA docosahexaenoic acid (DHA) that enhanced the efficacy of pembrolizumab in humanized NSCLC immune-xenografts. We suggest that PUFA enrichment in membrane phospholipids improves the efficacy of ICIs. We propose to repurpose letrozole or DHA as new immune-sensitizing agents in NSCLC.

1. Introduction

Lung cancer is one of the most common and deadly cancer types, with about 85 % of cases being non-small cell lung cancer (NSCLC) [1]. NSCLC treatment is based on surgical resection whenever possible, chemotherapy, target therapy and, recently, immunotherapy based on immune checkpoint inhibitors (ICIs), namely anti-programmed death-1 (anti-PD-1; pembrolizumab, nivolumab) and anti-programmed death-1 ligand-1 (anti-PD-L1; atezolizumab). Although the introduction of immunotherapy improved NSCLC patients' outcome, only 25 % of patients treated with ICIs have durable cancer remission, with many patients only partially responding or not responding at all [2]. PD-L1 is not

Abbreviations: NSCLC, non-small cell lung cancer; ICIs, immune checkpoint inhibitors; PD-1, programmed death-1; PD-L1, programmed death-1 ligand-1; PUFA, polyunsaturated fatty acid; MUFA, monounsaturated fatty acid; SFA, saturated fatty acid; DHA, docosahexaenoic acid; FBS, fetal bovine serum; DMSO, dimethyl sufoxide; PA, palmitic acid; BSA, bovine serum albumin; APC, allophycocyanin; ACLY, ATP citrate lyase; ACC, acetyl-coenzyme A carboxylase; FASN, FA synthase; SCD1/2, stearoyl-CoA desaturase 1/2; SREBP1, sterol regulatory element binding protein 1; TCR, T cell receptor; MDA, malonyl dialdehyde; NSG, NOD-scid-IL2Rγc$^{(-/-)}$; i.p., intraperitoneally; TIL, tumor-infiltrating lymphocyte; ANOVA, one-way analysis of variance; SPSS, Statistical Package for Social Science; PFS, progression-free survival; OS, overall survival; PLs, phospholipids; SCFA, short chain fatty acid; MCFA, medium chain fatty acid; LCFA, long chain fatty acid; NK, natural killer.

☆ **Twitter handle:** Letrozole and ω3-PUFA docosahexaenoic acid sensitizes non-small cell lung cancer to pembrolizumab.

* Corresponding author. Department of Oncology, University of Torino, piazza Nizza 44, 10126, Torino, Italy.
E-mail address: chiara.riganti@unito.it (C. Riganti).

[1] Current address: Department of Chemical Biology, Susan Lehman Cullman Laboratory for Cancer Research - Ernest Mario School of Pharmacy, Rutgers University, Piscataway, NJ.

[2] Stem Cell Immunity Team & Translational Immunotherapy Team - INSERM U932 - Institut Curie, Paris, France.

[3] Equal contributions.

https://doi.org/10.1016/j.canlet.2024.217221
Received 7 May 2024; Received in revised form 23 July 2024; Accepted 30 August 2024
Available online 6 September 2024

a strong predictive marker since high PD-L1 expression is not always associated to treatment benefit; conversely, a minimal expression of PD-L1 does not preclude a response [3].

Another factor challenging ICI's efficacy in NSCLC patients is biological sex, with important discrepancies in clinical response between male and female patients [4–6]. Estrogen receptors (ER) α and β, and autocrine production of 17-β-estradiol by aromatase are found in NSCLC [7] [8]: estrogens stimulate tumor progression [9], impair the response to cisplatin [10] and EGFR inhibitors [11], and affect the composition of the immune-infiltrate [12]. We previously demonstrated that ERα transcriptionally up-regulates PD-L1 in NSCLC and that patient-derived xenografts with high levels of β-estradiol/ERα axis are less responsive to pembrolizumab. On the other hand, this phenotype has the greatest benefit from the combination of ICI with the aromatase inhibitor letrozole, that down-regulates PD-L1 [13].

Besides inhibiting the extra-ovarian synthesis of estrogens, aromatase inhibitors affect the lipid cellular composition, altering the polyunsaturated fatty acids/monounsaturated + saturated fatty acid (PUFA/MUFA + SFA) ratio [14]. In colon, urothelial and lung murine tumors an increased PUFA/SFA ratio is associated to enhanced sensitivity to anti-PD-1 treatment [15], but the mechanisms are not clarified yet.

In this work, we have investigated whether letrozole improves the sensitivity to pembrolizumab by altering the FA composition in plasma membrane and the consequent binding between PD-L1 and PD-1. Our results indicated that either letrozole or a supplementation with long chain PUFAs as docosahexaenoic acid (DHA) enhances ICI efficacy in NSCLC by changing the membrane physic-chemical properties.

2. Materials and methods

2.1. Chemicals and materials

Fetal bovine serum (FBS) and culture medium were from Invitrogen Life Technologies (Carlsbad, CA). Plasticware for cell cultures was from Falcon (Becton Dickinson, Franklin Lakes, NJ). If not otherwise specified, the reagents were purchased by Sigma-Merck-Millipore.

2.2. Cell lines

Human NSCLC cell lines were purchased from ATCC (Manassas, VA, USA; Supplementary Table S1) and maintained in the respective culture media, with 10 % v/v FBS, 1 % v/v penicillin-streptomycin and 1 % v/v glutamine. All cell lines were authenticated by microsatellite analysis (PowerPlex kit; Promega, Madison, WI, USA; last authentication: October 2023). *Mycoplasma* spp. contamination was checked every 2 weeks by RT-PCR; contaminated cells were discharged. Letrozole was dissolved in dimethyl sufoxide (DMSO) and added in the culture medium maintaining a final concentration of DMSO ≤0.1 % v/v. Palmitic acid (PA) or DHA, dissolved in 90 % v/v ethanol, were added as 3:1 mix of FA/bovine serum albumin (BSA) to the culture medium, maintaining a final concentration of ethanol ≤0.1 % v/v. Untreated cells received DMSO or ethanol/BSA (vehicle) at the same concentrations.

2.3. Aromatase (CYP19A), EGFR kinase and Akt activity, 17-β-estradiol and testosterone measurement

Aromatase activity, EGFR kinase activity, Akt kinase activity, 17-β-estradiol and testosterone levels were measured using: Aromatase (CYP19A) Activity Assay Kit (#ab 273306, Abcam, Cambridge, UK), EGFR Kinase Assay kit (Promega), TruLight Akt1/PKBα Kinase Assay kit (Merck), Human Estradiol E2 ELISA Kit (ab285329, Abcam), Testosterone ELISA Kit (ab108666, Abcam), with a Synergy HTX-96 well reader (Bio-Tek Instruments, Winooski, VT).

2.4. Lipidome analysis

Samples were prepared using the automated MicroLab STAR® system (Hamilton, Reno, Nevada) and homogenized in deionized water. An aliquot of each homogenate was used for protein quantifications, the remaining part was subjected to a modified Bligh-Dyer extraction using methanol/water/dichloromethane in the presence of internal standards. The extracts were concentrated under nitrogen and reconstituted in 0.25 mL of 10 mM ammonium acetate in dichloromethane:methanol (50:50). The extracts were analyzed by liquid chromatography with nano PEEK tubing and Sciex SelexIon-5500 QTRAP (Shimadzu, Kyoto, Japan), via both positive and negative mode electrospray. The 5500 QTRAP scan was performed in MRM mode (≥1100 MRMs in total). Individual lipid species were quantified by considering the peak area ratios between target compounds and matched internal standards, multiplied per concentration of the internal standard. Raw data (available at https://portal.metabolon.com/and in the Supplementary Table S2) were extracted, peak-identified and quality-checked processed using Metabolon software (Morrisville, NC).

2.5. Flow cytometry

1×10^4 cells were washed in PBS, fixed with 4 % v/v paraformaldehyde for 5 min, incubated 15 min with an anti-CD274/PD-L1-allophycocyanin (APC)-conjugated antibody (clone29E.2A3; BioLegend, San Diego, CA; 1/50), and washed three times with PBS-FBS 1 %, then analyzed with a Guava® easyCyte flow cytometer (Millipore, Billerica, MA) using InCyte software (Millipore).

2.6. Immunoblot

Whole cell lysates were prepared in MLB buffer (125 mM Tris-HCl, 750 mM NaCl, 1 % v/v NP40, 10 % v/v glycerol, 50 mM $MgCl_2$, 5 mM EDTA, 25 mM NaF, 1 mM $NaVO_4$, 10 mg/ml leupeptin, 10 mg/ml pepstatin, 10 mg/m1 aprotinin, and 1 mM phenylmethylsulfonyl fluoride; pH 7.5), sonicated, and centrifuged at 13,000×*g* for 10 min at 4 °C. 30 μg of whole cell lysate proteins were probed with antibodies for: ATP citrate lyase (ACLY; #15421-1-AP, ProteinTech, Rosemont, IL; 1/2000), acetyl-coenzyme A carboxylase (ACC; #3662, Cell Signaling Technology, Danvers, MA; 1/1000), FA synthase (FASN; #3189, Cell Signaling Technology; 1/1000), stearoyl-CoA desaturase 1 (SCD1; #2438, Cell Signaling Technology; 1/1000), sterol regulatory element binding protein 1 (SREBP1; sc-13551, Santa Cruz Biotechnology Inc., Santa Cruz, CA, recognizing the uncleaved protein; 1/500), phospho(Thr202/Tyr204)ERK1/2 (#9101, Cell Signaling Technology; 1/1000), ERK1/2 (#4696, Cell Signaling Technology; 1/1000), Ras (#415700, ThermoFisher Scientific, Waltham, MA; 1/1000), epidermal growth factor receptor (EGFR; #MA5-13269, ThermoFisher Scientific; 1/1000), anti-β-tubulin (sc-5274, Santa Cruz Biotechnology Inc.; 1/1000) antibodies. 20 μg of whole cell lysate were subjected to a pull-down assay to measure Ras-GTP, an index of active Ras, using the Active Ras Pull-Down and Detection Kit (1611, ThermoFisher Scientific) as per manufacturer's instructions. Nuclear extracts were prepared using a Nuclear Extract kit (Active Motif, La Hulpe, Belgium). 10 μg of nuclear proteins were immunoblotted with anti-SREBP1c (#NB100-2215, Novus Biologicals, Centennial, CO, recognizing the cleaved and transcriptionally active fragment only; 1/500) or anti-TFIID/TATA box-binding protein (TBP) (58C9, Santa Cruz Biotechnology Inc.; 1/250) antibodies. The proteins were detected using enhanced chemiluminescence (Gel Doc and Image Lab Touch Software, Bio-Rad Laboratories).

2.7. RT-PCR

Total RNA was extracted and reverse-transcribed using an iScript™ cDNA Synthesis Kit (Bio-Rad Laboratories, Hercules, CA). RT-PCR was performed using the IQ SYBR Green Supermix (Bio-Rad Laboratories).

Primer sequences are listed in Supplementary Table S3. Relative quantitation was performed with the Bio-Rad Software Gene Expression Quantitation.

2.8. Cell viability

5×10^4 cells were seeded in a 96-well plate. After 24 h, cells were incubated with different concentrations of the test compounds. The viability was measured after 48 h using the colorimetric WST-1 based assay (Roche Diagnostics, Mannheim, Germany). Results were expressed as a percentage of viable cells vs. untreated cells (considered as 100 %). IC50, IC25 and IC10 were calculated with the GraphPad software.

2.9. Membrane fluidity, DHA and PA quantification

Membrane fluidity was measured fluorometrically using the Membrane Fluidity Kit (#ab189819, Abcam). DHA was measured spectrophotometrically with the Docosahexaenoic Acid ELISA Kit (abx258057, Abbexa, Cambridge, UK). PA was measured as in paragraph 2.4.

2.10. In vitro PD-1/PD-L1 binding assay

5×10^3 HEK-293 cells were seeded into 96-well plates and transiently transfected with PD-L1 and T cell receptor (TCR), using the components of the PD-1:PD-L1/PD-L2 Cell-Based Inhibitor Screening Assay Kit (BPS Bioscience, San Diego, CA). HEK-293 cells were co-incubated at 1:1 ratio overnight with growth-arrested PD-1/NFAT reporter-Jurkat cells, constitutively transfected with luciferase (BPS Bioscience). NFAT-luciferase activation was inhibited when PD-1 was bound by PD-L1, and increased when the binding decreased. The chemiluminescence units were an index of PD-1/PD-L1 binding.

2.11. Malonyl dialdehyde (MDA) measurement

The amount of MDA, an index of lipid peroxidation, was measured in cell lysates with the Lipid Peroxidation (MDA) Assay Kit (ab118970, Abcam), as per manufacturer's instructions.

2.12. In vivo experiments

1×10^6 A549, NCI-H1385, NCI-H1650 and NCI-H1975 cells, mixed with 100 μl matrigel, were injected subcutaneously in 16-week female NOD-scid-IL2Rγc$^{(-/-)}$ (NSG) mice engrafted with human cord blood-derived hematopoietic CD34$^+$ cells (Hu-CD34$^+$; The Jackson Laboratories, Bar Harbor, MA, stock #005557). This mice strain has a stable engraftment of human functional immune cells, without the occurrence of a graft-versus host-disease. Circulating immune cells include CD4$^+$/CD8$^+$lymphoid cells with a strong diversity of T-cell receptor repertoire [16], and myeloid cells such as monocytes, bone-marrow-derived macrophages and neutrophils [17]. The mice used in the study were engrafted with hematopoietic CD34$^+$ cells from 8 different human donors; the mice from different donors were randomized between each experimental setting. At the baseline mice showed comparable weight and immunophenotypes (Supplementary Table S4). Animals were housed (5 per cage) under 12 h light/dark cycle, with food and drinking provided *ad libitum*. Tumor growth was measured daily by caliper, according to the equation $(LxW^2)/2$, where L = tumor length and W = tumor width. When tumor reached the volume of 100 mm^3, mice were randomized in the following groups: 1) Vehicle group, treated intraperitoneally (i.p.) with 100 μl saline solution (days 1, 7, 14, 21, 28, 35 after randomization); 2) pembrolizumab group, treated with 10 mg/kg i.p. of 100 μl saline solution of the drug (day 1), followed by 5 mg/kg i.p. (days 7, 14, 21, 28, 35); 3) docosahexaenoic acid (DHA) group, treated with 100 μl of DHA (44.5 % v/v in sesame oil) *per os* daily (days 1–35); 4) pembrolizumab + DHA group. Mice were euthanized on day 40 with zolazepam (0.2 ml/kg) and xylazine (16 mg/kg). In a second set, animals were treated until day 35 and left untreated to monitor progression free survival (PFS) and overall survival (OS). In a third set, animals were treated with 100, 50 and 25 μl of DHA (corresponding to 44.5 %, 22.25 % and 11.12 % v/v in sesame oil) *per os* daily (days 1–35), associated with pembrolizumab as above. In all the experimental conditions with DHA, alone or with pembrolizumab, we did not register any death during the protocol. The experimental procedures were approved by the local Bio-Ethical Committee and by the Italian Ministry of Health (#627/2018-PR, 10/08/2018).

2.13. Tumor cells and tumor-infiltrating lymphocyte (TIL) analysis

Resected tumors were digested with 1 mg/ml collagenase and 0.2 mg/ml hyaluronidase (1 h at 37 °C), and filtered using a 70 μm-cell strainer to obtain a single cell suspension. Tumor cells, isolated with the Tumor Cell Isolation Kit (Miltenyi Biotec., Bergisch Gladbach, Germany), were stained with an anti-CD274/PD-L1 antibody (29E.2A3; BD Pharmingen, San Diego, CA). Tumor-infiltrating lymphocytes (TILs), isolated with the Pan T Cell Isolation kit (#130-096-535; Miltenyi Biotec.), were stained with the following antibodies (Miltenyi Biotec., dilution 1/10): anti-CD8 (BW135/80), anti-CD56 (AF127H3), anti-TCR Vγ9 (REA470), anti-Ki67 (REA183), anti-INF-γ (REA600). Cells were quantified using a Guava® easyCyte flow cytometer and InCyte software. Results were expressed as percentage of CD8$^+$Ki67$^+$IFNγ$^+$cells over CD8$^+$cells, CD56$^+$Ki67$^+$IFNγ$^+$cells over CD56$^+$cells, Vγ9$^+$Ki67$^+$IFNγ$^+$over Vγ9$^+$cells.

2.14. Statistical analysis

All data are provided as means ± SD. The results were analyzed by a one-way analysis of variance test (ANOVA), using Statistical Package for Social Science (SPSS) software (IBM SPSS Statistics v.19). $p < 0.05$ was considered significant. The sample size for animal studies was calculated with the G*Power software (www.gpower.hhu.de), setting $\alpha < 0.05$ and $1\text{-}\beta = 0.80$. Progression-free survival (PFS) was defined as the time from the starting of treatment to the time of ≥10 % of increase in tumor volume in three consecutive measures. Overall survival (OS) was defined as the time from the starting of treatment to death. The Kaplan-Meier method was used to calculate PFS and OS. Log-rank test was used to compare the outcomes of each group.

3. Results

3.1. NSCLC cells have variable aromatase activity and production of 17-β-estradiol

In a screening of 29 NSCLC cell lines, derived from patients of different genders, stage, histotype and smoking history (Supplementary Table S1) and recapitulating the resistance/sensitivity to ICI of real patients [13], we found a great variability in the endogenous aromatase activity (Fig. 1A). We focused on the two cell lines with the lowest (A549, NCI-H1385) and highest (NCI-H1650, NCI-H1975) aromatase activity. Letrozole significantly reduced the enzymatic activity (Fig. 1B) and the production of 17-β-estradiol (Fig. 1C), with greatest effects in cells with high aromatase activity and 17-β-estradiol synthesis (NCI-H1650, NCI-H1975, defined as "letrozole responders") than in cells with low activity of aromatase and production of 17-β-estradiol (A549, NCI-H1385, defined as "letrozole non-responders"). Consistently with previous findings [13], the surface PD-L1 levels followed this rank order: A549<NCI-H1385<NCI-H1650<NCI-H1975. Letrozole reduced PD-L1 amount in the letrozole-responder cell lines (Fig. 1D).

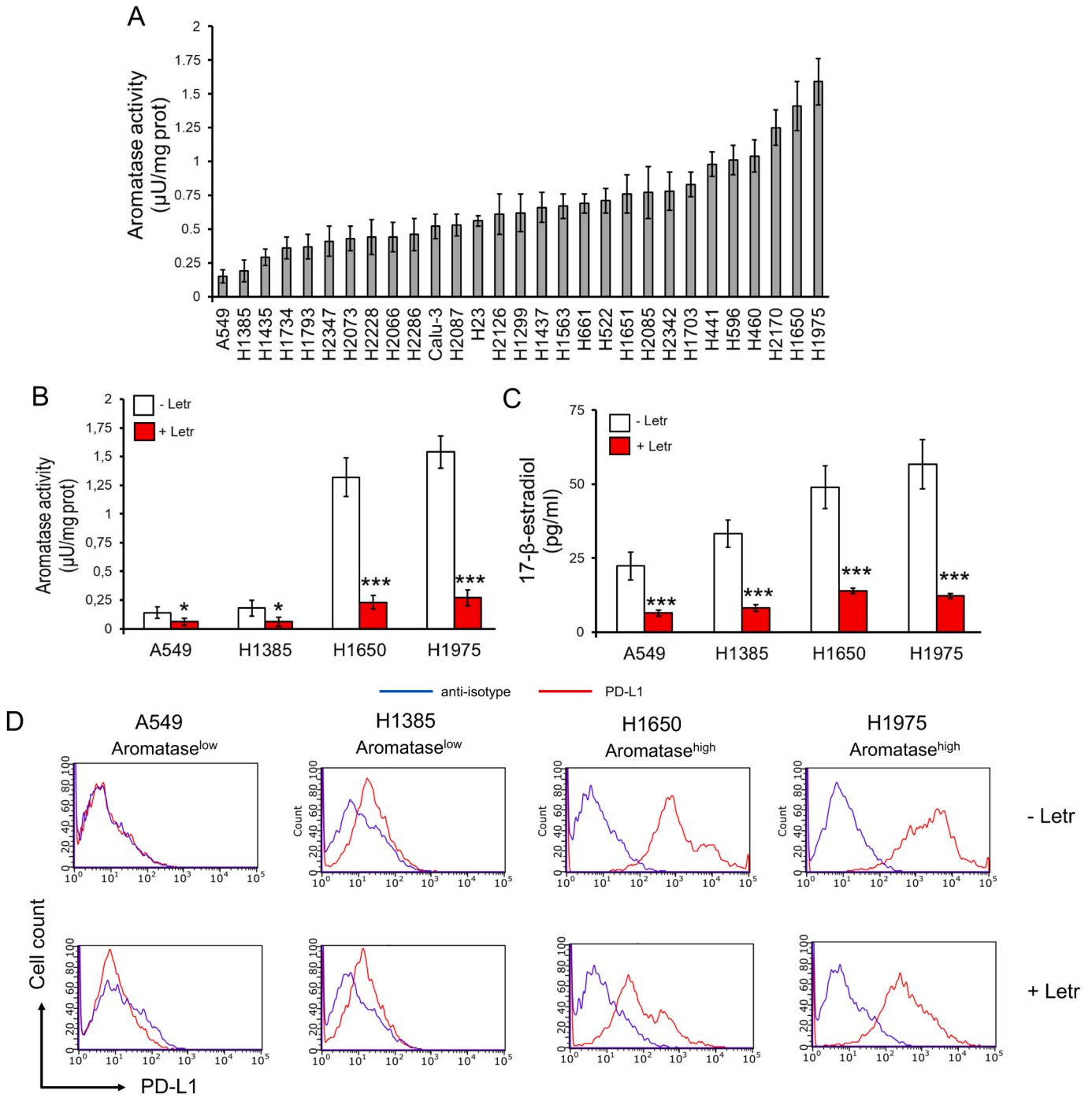

Fig. 1. Aromatase activity and 17-β-estradiol production in NSCLC cells. (**A**) Aromatase activity in 29 NSCLC cell lines, measured by ELISA. Data are shown as the mean ± SD (n = 3 independent experiments, with technical duplicates). (**B-D**) Cells were treated 24 h with (+) or without (−) letrozole (Letr; 10 nM) for 24 h "- Letr" cells: cells grown in fresh medium containing 0.1 % v/v DMSO. Aromatase activity (**B**) and 17-β-estradiol production (**C**) were measured by ELISA in duplicates. Data are shown as the mean ± SD (n = 3 independent experiments, with technical duplicates). *p < 0.05, ***p < 0.001 treated vs untreated cells. (**D**) Surface PD-L1 level, measured by flow cytometry in duplicates. When indicated, cells were stained with an anti-isotype antibody, as internal control. The image is representative of 1 out of 3 experiments.

3.2. Letrozole reshapes membrane PUFA/MUFA + SFA ratio in non-small cell lung cancer cells by activating SREBP1c and up-regulating lipogenic genes

As far as lipidome is concerned, we noticed a progressive enrichment in phospholipids (PLs), ceramides and cholesterol, key components of plasma membrane, moving from poor to good letrozole-responder cells, but no significant changes in neutral lipids (mono-, di- and triacylglycerols) (Fig. 2A; Supplementary Table S2). Letrozole moderately increased the amount of short chain and medium chain FAs (SCFAs, MCFAs) in responder cells. For long chain FAs (LCFAs), letrozole did not change SFAs, MUFAs and PUFAs in non-responder cells, but it increased these species in responder cells (Fig. 2B; Supplementary Table S2), thereby increasing the PUFA + MUFA/SFA ratio in the main PLs contained in the plasma membrane (Fig. S1). Narrowing the focus on the PL species significantly up-regulated, in the less responsive cells

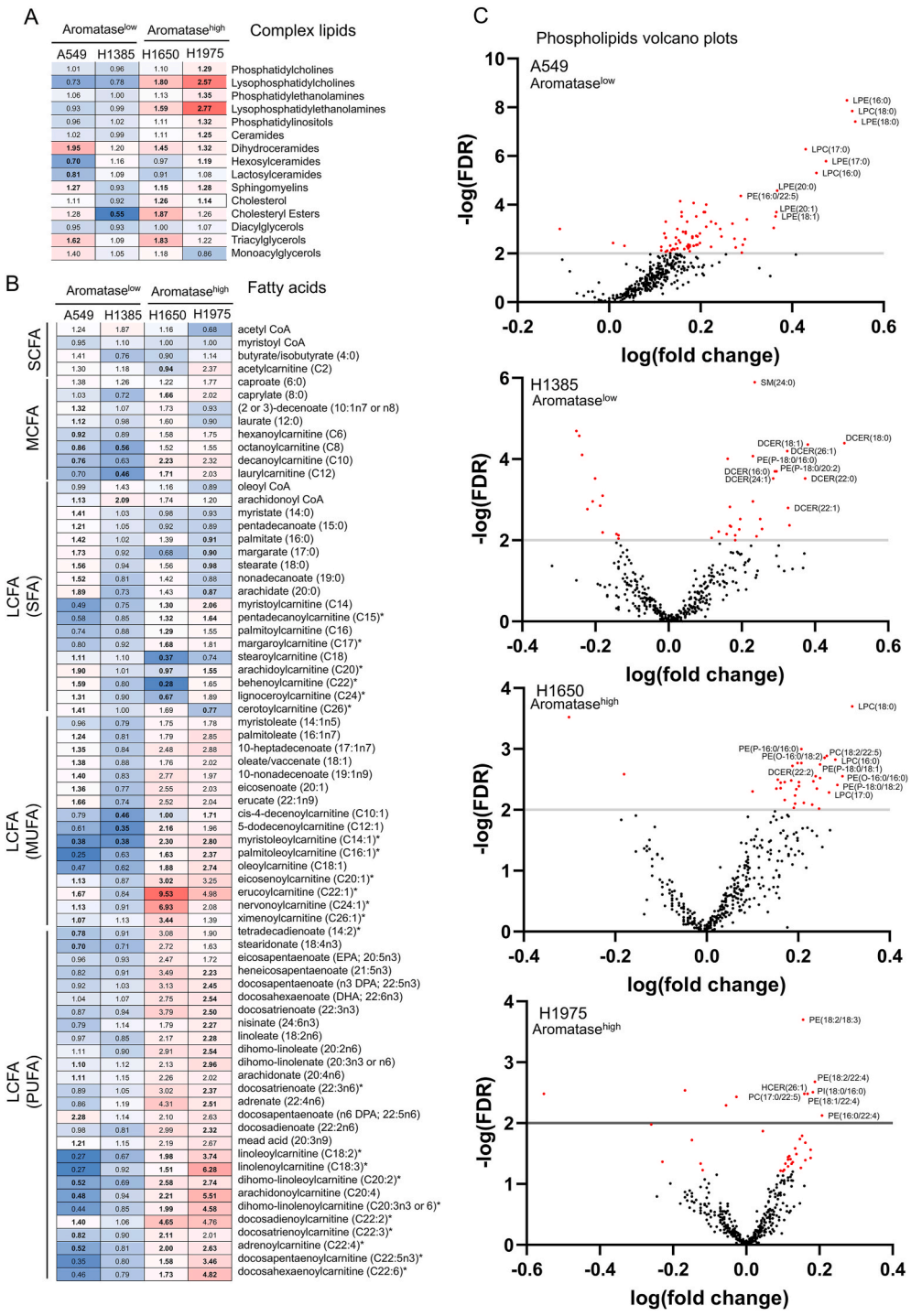

Fig. 2. Lipidomic profile of NSCLC cells. Cells were treated with or without letrozole (10 nM) for 24 h, then used for lipidomic analyses. Untreated cells were grown in fresh medium containing 0.1 % v/v DMSO. (**A-B**) Heatmap of complex lipids (**A**) and fatty acids (**B**). Data are mean scaled intensity for a metabolite in letrozole-treated cells versus untreated cells (n = 5 independent experiments). SCFA: short chain fatty acids; MCFA: medium chain fatty acids; LCFA: long chain fatty acids; SFA: saturated fatty acids; MUFA: monounsaturated fatty acids; PUFA; polyunsaturated fatty acids. Red: upregulated lipids; blue: downregulated lipids; bold: statistically significant results. (**C**) Volcano plots of significantly up- and down-regulated phospholipids (red circle) in letrozole-treated cells versus the untreated cells (n = 5 independent experiments).

(A549), letrozole increased 7 SFA-containing PLs and 3 MUFA/PUFA-containing PLs. In NCI-H1385 cells we detected the increase of 5 SFA-containing and 4 MUFA-containing PLs. Moving to the more responsive cells, 4 SFA-containing PLs and 5 MUFA/PUFA-containing PLs (NCI-H1650 cells), 1 SFA-containing PL and 6 MUFA/PUFA-containing PLs (NCI-H1975) were increased (Fig. 2C).

This pattern may be explained by higher lipogenesis and/or lipid remodelling induced by letrozole.

To clarify this point, we measured mRNA and protein levels of SREBP1 and its target genes *ACLY*, *ACC*, *FASN*, *SCD1* and *SCD2* [18,19]. *ACLY*, *FASN* and *SCD1*, which are master regulators in the synthesis and desaturation of FAs, were higher in letrozole responder NCI-H1650 and NCI-H1975 cells than in letrozole non-responder A549 and NCI-H1385 cells, at both mRNA (Fig. 3A) and protein (Fig. 3B) level. Interestingly,

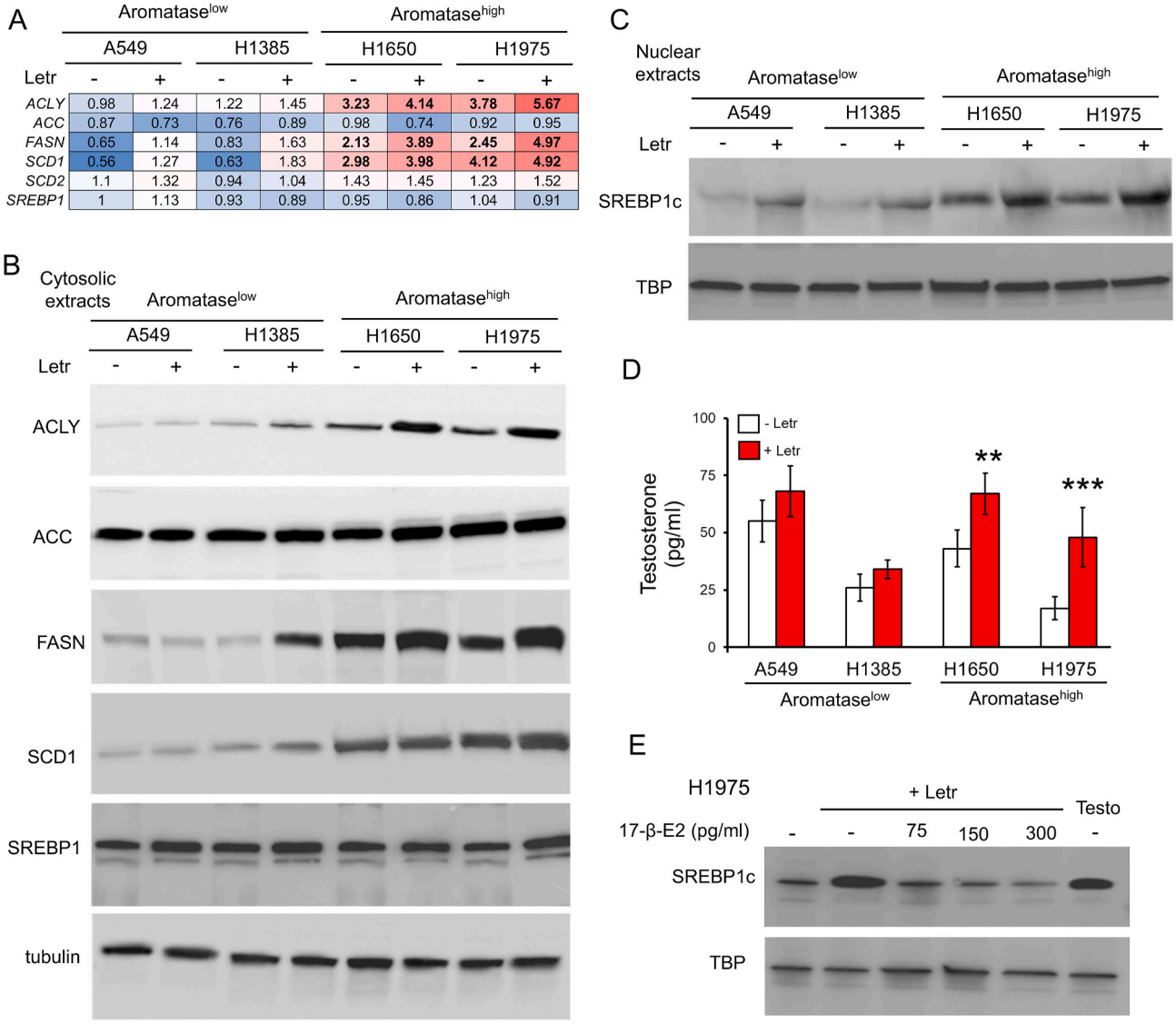

Fig. 3. Letrozole up-regulates lipogenic genes by activating SREBP1c in a testosterone-dependent way. Cells were treated with (+) or without (−) letrozole (Letr; 10 nM) for 24 h. Untreated cells were grown in fresh medium containing 0.1 % v/v DMSO. (**A**) Heatmap of lipogenic genes, measured by qRT-PCR. Data are the mean of normalized gene expression in letrozole-treated cells versus untreated cells (n = 3 independent experiments, in technical triplicates). Red: upregulated genes; blue: downregulated genes; bold: statistically significant results. (**B**) Immunoblotting of the indicated proteins in cytosolic extracts. Tubulin has been used as a control of equal protein levels. The image is representative of 1 out of 3 experiments. (**C**) Immunoblotting of SREBP1c (cleaved, transcriptionally active fragment) in nuclear extracts. TBP has been used as a control of equal protein levels. The image is representative of 1 out of 3 experiments. (**E**) Testosterone levels, measured by ELISA. Data are shown as the mean ± SD (n = 3 independent experiments, in technical duplicates). **p < 0.01, ***p < 0.001: - Letr vs + Letr cells. (**F**) NCI-H1975 cells were grown 24 h in fresh medium (−), in medium containing 10 nM letrozole (+Letr), alone (−) or in the presence of increasing concentrations (75, 150, 300 pg/ml) of 17-β-estradiol, or in medium containing 50 pg/ml testosterone (Testo, -). The amount of SREBP1c was measured in nuclear extracts by immunoblotting. TBP has been used as a control of equal protein levels. The image is representative of 1 out of 3 experiments.

letrozole further increased *FASN, ACLY* and *SCD1* expression. By contrast SREBP1 mRNA and cytosolic protein, corresponding to the uncleaved, transcriptionally inactive SREBP1, were unchanged across cell lines, with and without letrozole (Fig. 3A–B). The nuclear traslocated, transcriptionally active form of SREB1c was higher in letrozole responder than in letrozole non-responder cells, and was increased by letrozole (Fig. 3C). Mechanistically, letrozole increased the intracellular testosterone accumulation (Fig. 3D), by preventing its aromatization into 17-β-estradiol. It has been reported that testosterone is the endogenous activator of SREBP1c cleavage [20]. In letrozole responder NCI-H1975 cells testosterone increased the amount of nuclear SREBP1c, mimicking the effects of letrozole, while 17-β-estradiol abrogated letrozole effect on SREBP1c cleavage/activation (Fig. 3E).

SREBP1c in mouse lung cancer engineered to express mutated KRAS is up-regulated by KRAS/ERK2 axis [21], and in liver cancer it is up-regulated by the EGFR/Akt axis [18]. Since A549 cells were KRAS mutated [p.Gly12Ser (c.34G > A)], NCI-H1650 cells were EGFR mutated [p.Glu746-Ala750del (c.2235_2249del15)], NCI-H1975 cells were KRAS mutated [p.Gly12Asp (c.35G > A)] and EGFR mutated [p.Thr790Met (c.2369C > T), p.Leu858Arg (c.2573T > G)], implying a higher activity of Ras- and EGFR-dependent pathways, we investigated if letrozole's effects on SREBP1c and lipogenic genes could be mediated by changes in these axes. Consistently with the mutational profile, Ras activity was higher in A549 and NCI-H1975 cells (Fig. S2A). The activity of ERK1/2, which is a downstream effector of Ras [21] and EGFR [13], was higher in A549, NCI-H1650 and NCI-H1975 cells (Fig. S2A). Despite the comparable amount of EGFR in all cell lines (Fig. S2B), the activity of EGFR (Fig. S2C) and downstream effector Akt (Fig. S2D) was lower in

wild-type EGFR cells (A549, NCI-H1385) and higher in mutated EGFR cells (NCI-H1650, NCI-H1975). Letrozole did not change the activity of RAS, ERK1/2, EGFR or Akt (Figs. S2A–D). Moreover, in NCI-H1975 cells, characterized by the higher Ras and EGFR activity, the inhibitors of EGFR (AZD9291), ERK1/2 (U-0126) or Akt (MK-2206), used at concentrations that completely abrogated the kinase activities [13], did not change the expression of *SREBP1*, *ACLY*, *FASN, SCD1* and *SCD2* toward the baseline (Fig. S2E). These results suggest that the effects of letrozole on SREBP1c in human NSCLC cell lines were independent from Ras/ERK1/2 and EGFR/Akt axes.

3.3. Letrozole reduces PD-1/PD-L1 binding by increasing membrane fluidity

We next evaluated whether the changes in FAs induced by letrozole via the activation of SREBP1c alter the physic-chemical properties of plasma membrane as consequence of altered lipidome composition [14]. Non-toxic concentrations of letrozole (Fig. S3A), sufficient to inhibit the aromatase activity (Fig. 1B), produced a moderate increase of membrane fluidity in non-responder (A549, NCI-H1385) cells that became significant in responder (NCI-H1650, NCI-H1975) cells and in HEK293 cells overexpressing PD-L1 (Fig. 4A). To prove that such increase in membrane fluidity alters PD-L1 interaction with PD-1, we measured the PD-L1/PD-1 binding in HEK293 cells stably overexpressing PD-L1 and a TCR activator, co-incubated with NFAT-luciferase transduced-Jurkat cells expressing PD-1 and TCR (Fig. 4B). Interestingly, letrozole decreased the PD-L1/PD-1 binding in this system (Fig. 4C).

3.4. A high PUFA/SFA ratio reduces PD-1/PD-L1 binding, phenocopying letrozole

As second proof that the effect of letrozole on the reduced PD-L1/PD-1 binding was caused by altered plasma membrane composition and fluidity, we supplemented NSCLC and HEK293 cells with the SFA PA and the PUFA DHA, at concentrations corresponding to their IC50 for each cell line (Fig. S3B). Although the cell lines analyzed had different contents of PA and DHA, in basal condition and after supplementation, the incorporation of the two FAs was the same, since the enrichment ([FA] after supplementation/[FA] in basal condition) was similar (Fig. 5A). As expected, PA-treated cells decreased and DHA-treated cells increased membrane fluidity (Fig. 5B), mimicking the effect of letrozole. Accordingly, PA increased and DHA reduced the PD-L1/PD-1 binding in the HEK293/T-Jurkat system (Fig. 5C).

Recently, it has been reported that the inhibition of FASN synergizes with anti-PD-L1 inhibitors by increasing MHC1 protein exposed on liver cancer cells [22]. In NSCLC cells we also observed an immuno-sensitizing effect, although the mechanisms was different. Indeed, the FASN inhibitor Orlistat, at a concentration that reduces the enzyme activity of >75 % in NCI-H1975 cells [23], significantly decreased the content of PA in the NSCLC tested, as well as in PD-L1-overexpressing HEK293 cells, while it produced minor changes in the content of DHA (Fig. 5D). As a results, Orlistat-treated cells had increased DHA/PA ratio (Fig. 5E), increased membrane fluidity (Fig. 5F) and decreased binding between PD-L1 on HEK293 and PD-1 on T-Jurkat cells (Fig. 5G).

A high amount of PUFAs, which are easily oxidized, can lead to ferroptosis [24]. However, we did not find any increase in MDA, a typical product of lipid peroxidation, in cells treated with letrozole (Fig. S4A), DHA (Fig. S4B) or Orlistat (Fig. S4C), three conditions increasing PUFAs. These results exclude that the immunosensitization elicited by the lipidome-targeting agents is linked to the induction of ferroptotic cell death.

3.5. DHA enhances the efficacy of pembrolizumab in non-small cell lung cancer immune-xenografts

To verify the efficacy of DHA as enhancer of ICIs, as previously demonstrated by letrozole [13], we implanted NSCLC tumors in Hu-CD34^{+} mice. Tumors showed a progressive sensitivity to pembrolizumab that followed this rank order: A549<NCI-H1385<NCI-H1650<NCI-H1975. DHA alone did not reduce tumor growth (Fig. 6A), nor increase PFS or OS (Fig. 6B–C). The combination of pembrolizumab + DHA, however, reduced tumor growth and increased mice survival (Fig. 6A–C), with a progressively increasing

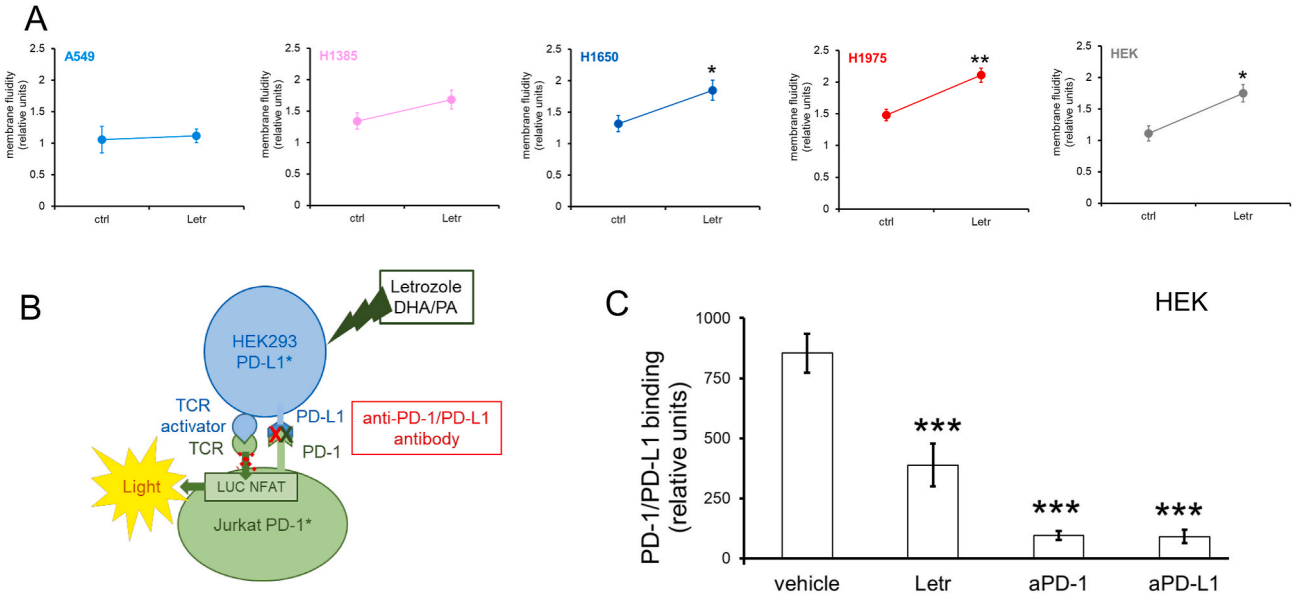

Fig. 4. NSCLC cell membrane fluidity determinates PD-L1/PD-1 binding. Cells were treated with fresh medium containing DMSO 0.1 % (ctrl) or letrozole (Letr; 10 nM) for 24 h (**A**) Membrane fluidity, measured fluorometrically. Data are shown as the mean ± SD (n = 3 independent experiments, in technical duplicates). *p < 0.05, **p < 0.01: Letr-treated vs ctrl cells. (**B**) Schematic representation of the PD-L1/PD-1 binding assay. (**C**) PD-L1/PD-1 binding, measured as chemiluminescence units produced by Jurkat cells, co-cultured with HEK293 cells pre-treated with (+) or without (−) letrozole (Letr; 10 nM) for 24 h. When indicated, the anti-PD-1 (αPD-1) and the anti-PD-L1 (αPD-L1) provided by the kit were added as positive controls. Data are shown as the mean ± SD (n = 3 independent experiments, in technical duplicates). ***p < 0.001: Letr-treated vs ctrl cells.

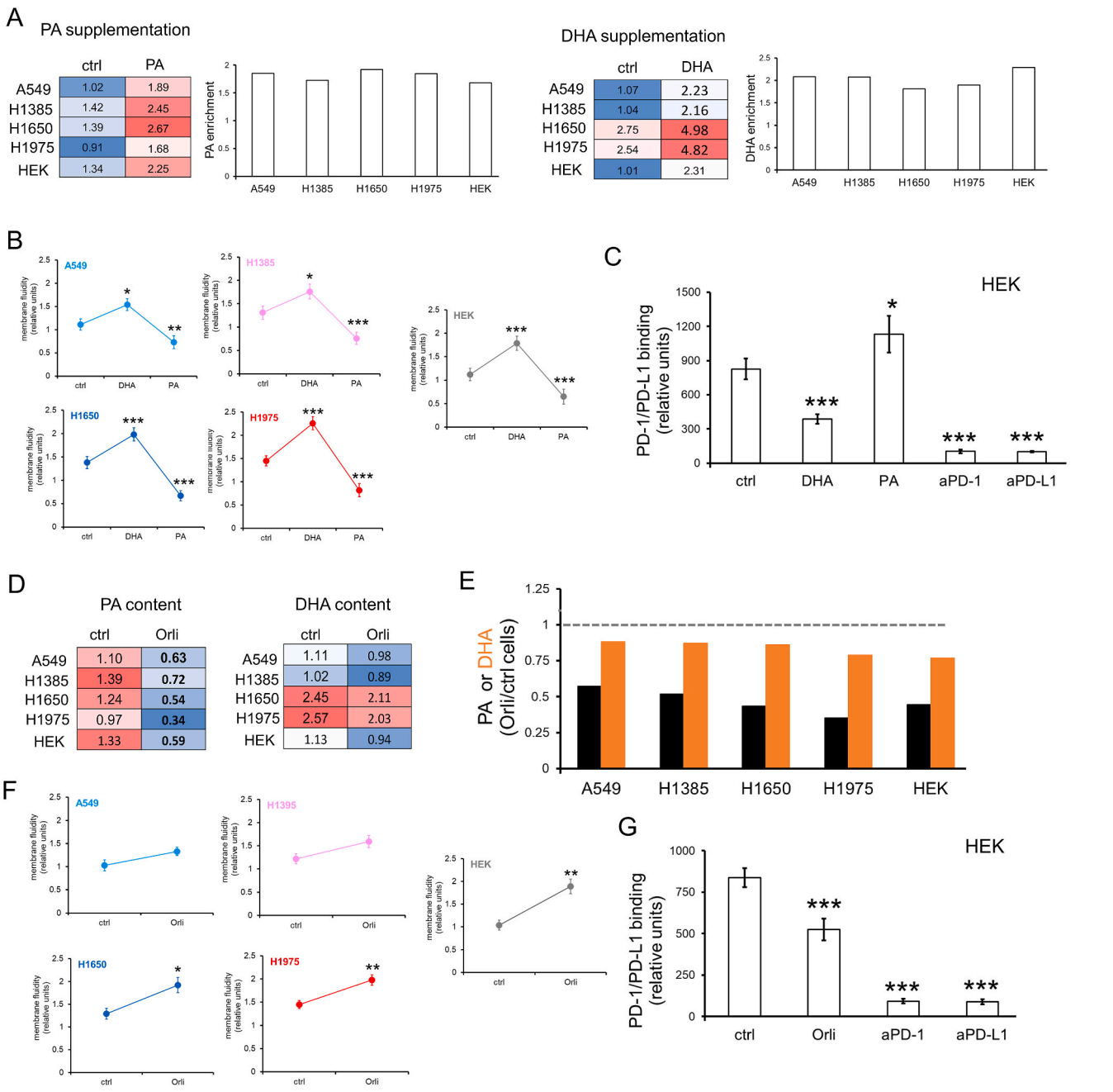

Fig. 5. The higher DHA/PA content increased membrane fluidity and impaired the PD-L1/PD-1 binding. Cells were treated with fresh medium containing BSA-ethanol 0.1 % v/v (ctrl), palmitic acid (PA) or docosahexaenoic acid (DHA) for 24 h at their respective IC50 for each cell line (Fig. S3B). (**A**) PA and DHA cellular content, measured by mass spectrometry or ELISA. Heatmaps are mean scaled intensity for PA or DHA in treated cells versus untreated (ctrl) cells (n = 3 independent experiments). Histograms showed the DHA/PA enrichment (amount of DHA or PA present in supplemented cells/amount of PA or DHA present in ctrl cells). (**B**) Membrane fluidity, measured fluorometrically. Data are shown as the mean ± SD (n = 3 independent experiments, in technical duplicates). *p < 0.05, **p < 0.01, ***p < 0.001: DHA/PA-treated vs ctrl cells. (**C**) PD-L1/PD-1 binding assay, using HEK293 cells pre-treated 24 h with DHA or PA at their IC50. Data are shown as the mean ± SD (n = 3 independent experiments). ***p < 0.001: DHA/PA-treated vs ctrl cells. (**D**) PA and DHA cellular content, measured by mass spectrometry or ELISA, in cells treated with 30 μM Orlistat (Orli) for 24 h. Heatmaps are mean scaled intensity of PA or DHA content in Orli-treated versus untreated (ctrl) cells (n = 3 independent experiments). Bold: statistically significant results. (**E**) Histograms representative of PA and DHAs content in Orlistat-treated cells vs. untreated (ctrl) cells. The content of PA and DHA in ctrl cells was considered 1 (dashed line). (**F**) Membrane fluidity, measured fluorometrically. Data are shown as the mean ± SD (n = 3 independent experiments, in technical duplicates). *p < 0.05, **p < 0.01: Orlistat-treated vs ctrl cells. (**G**) PD-L1/PD-1 binding assay, using HEK293 cells pre-treated 24 h with 30 μM Orlistat. Data are shown as the mean ± SD (n = 3 independent experiments). ***p < 0.001: Orli-treated vs ctrl cells.

efficacy, moving from letrozole non-responder tumors (A549, NCI-H1385) to letrozole responder tumors (NCI-H1650, NCI-H1975) [13]. The reduction in tumor volume as difference between the tumor volume in vehicle-treated group and the tumor volume in pembrolizumab + DHA-treated group at day 40 followed this order: A549<NCI-H1385<NCI-H1650<NCI-H1975, without however significant differences between letrozole non-responder and letrozole responder tumors (Fig. S5A). The sensitizing effect of DHA was dose-dependent: in letrozole non-responder tumors (A549, NCI-H1385) lower doses of DHA progressively lost their efficacy in rescuing pembrolizumab's efficacy, while low DHA doses had a decreased but still significant effect in letrozole responder tumors (NCI-H1650,

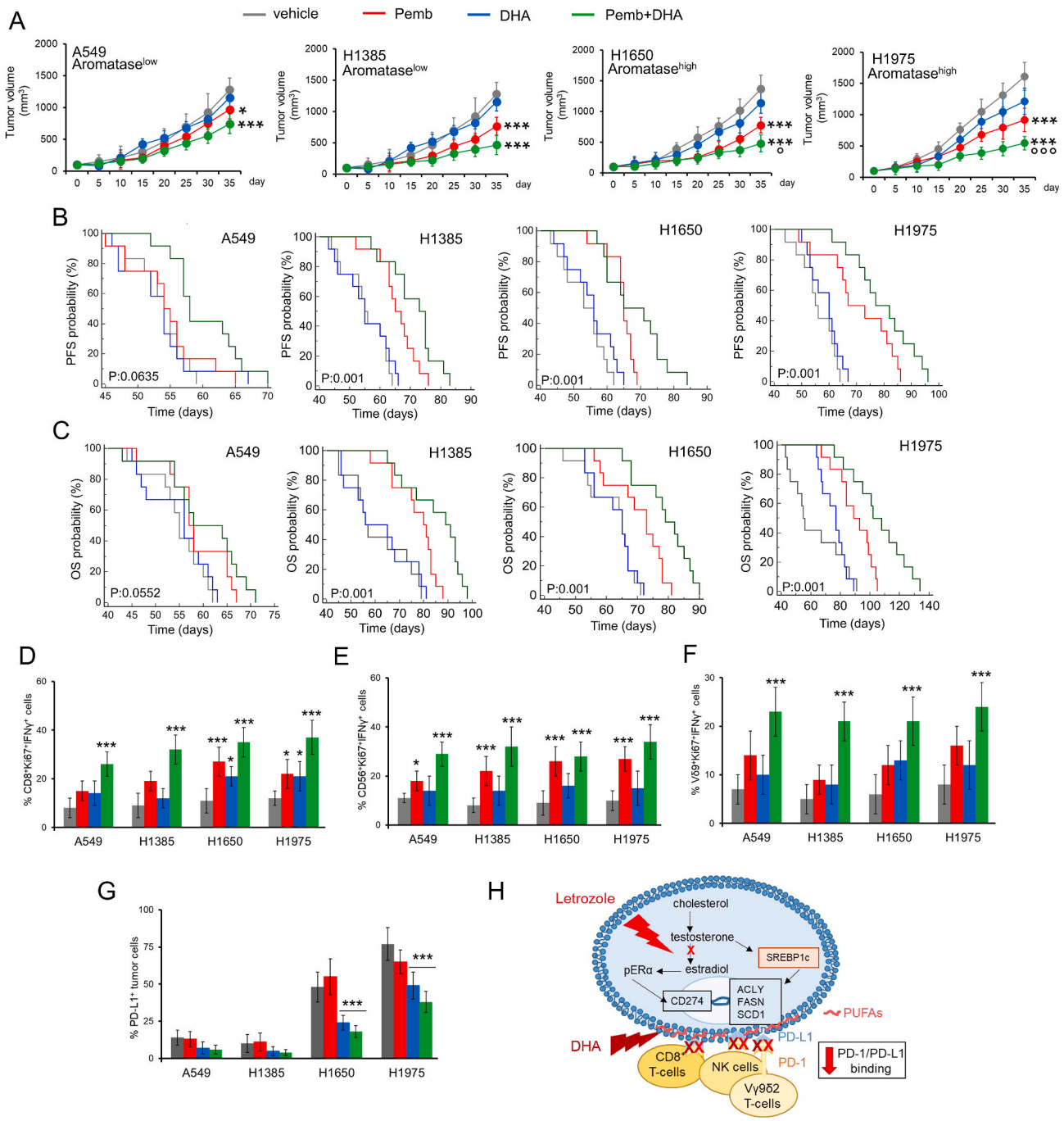

Fig. 6. DHA enhances the antitumor efficacy of pembrolizumab in NSCLC immune-xenografts. Hu-CD34$^+$ mice were injected subcutaneously with human 1 × 10^6 NSCLC cells (A549, NCI-H1385, NCI-H1650, NCI-H1975), mixed with 100 μl Matrigel. When tumor volume reached 100 mm^3, mice were randomized and treated with: vehicle (saline solution), pembrolizumab (Pemb), DHA or their combination (Pemb + DHA) for 35 days. (**A**) Tumor growth was monitored by a caliper and animals were euthanized at day 40. Data are shown as the mean ± SD (n = 10 mice/group). *p < 0.05, ***p < 0.001: treated groups vs vehicle group; °p < 0.05, °°°p < 0.001: Pemb + DHA-treated group vs Pemb-treated group. (**B, C**) PFS and OS of mice (n = 10 mice/group). ***p < 0.001: Pemb + DHA treated group versus vehicle treated group (for all the groups, except A549). (**D, E, F, G**) Percentage of intratumor CD8$^+$Ki67$^+$INFγ$^+$(**D**), CD56$^+$Ki67$^+$INFγ$^+$ (**E**), Vγ9$^+$Ki67$^+$IFNγ$^+$cells (**F**) and PD-L1$^+$ tumor cells (**G**), measured by flow cytometry on dissociated explanted tumors (n = 10 mice/group). *p < 0.05, ***p < 0.001: treated groups vs vehicle group. (**H**) Scheme of the immuno-sensitizing mechanisms of letrozole and DHA in non-small cell lung cancer.

NCI-H1975; Fig. S5B). Consistently, in HEK293 cells treated with DHA at IC25 and IC10 instead of IC50, the membrane fluidity progressively decreased (Fig. S5C) and the PD-L1/PD-1 binding progressively increased (Fig. S5D).

The antitumor efficacy of high dose DHA + pembrolizumab was paralleled by the increased infiltration, proliferation and activation of CD8$^+$T-lymphocytes (Fig. 6D), natural killer (NK) cells (Fig. 6E) and Vγ9Vδ2 T-cells (Fig. 6F), and by the decrease of PD-L1 on tumor cells (Fig. 6G). This immunophenotype phenocopied the effects of the combination of letrozole + pembrolizumab [13], suggesting that letrozole and DHA share a common immuno-sensitizing mechanism, based on the increased PUFA + MUFA/SFA ratio and fluidity in plasma membrane (Fig. 6H).

4. Discussion

The present work demonstrates for the first time that: i) letrozole impairs the binding of PD-L1 to PD-1, thereby improving the efficacy of ICIs in NSCLC, by altering the cellular phospholipidome and increasing the PUFA + MUFA/SFA ratio; ii) the supplementation with PUFAs recapitulates the immuno-sensitizing benefit produced by letrozole, representing a new approach in treating NSCLC unresponsive to anti-PD-1/anti-PD-L1 agents.

The screening of a panel of NSCLC cell lines, exhibiting different endogenous aromatase activity indicated that cells poorly responsive to the combination of letrozole + pembrolizumab had the lowest aromatase activity. The opposite was true for cells with the highest activity of aromatase, that benefitted the most from the combination letrozole + pembrolizumab [13]. This association is not tumor-dependent. Indeed, the levels of aromatase directly and inversely correlate with the amount of PD-L1 and infiltrating $CD8^{+}$T-lymphocytes, respectively, in colon cancer [25], suggesting that high aromatase levels are associated with more immuno-suppressive environment and lower sensitivity to ICIs.

Interestingly NSCLC patients with stable disease/partial response to anti-PD-1 had higher levels of phosphatidylglycerols, lysophosphatidylglycerols and phosphoinositides compared to patients with progressive disease [26]. This observation prompted us to investigate whether, beyond reducing the transcriptional level of PD-L1 [13], letrozole may also impact on the phospholipidome profile, altering the physic-chemical properties of plasma membrane, and impacting on the PD-L1 conformation and/or binding to PD-1. Indeed, in responder cells, letrozole increased phosphatidylcholine, lyso-phosphatidylcholine, phosphatidylethanolamine, lyso-phosphatidylethanolamine and phosphatidylinositol, recapitulating the phospholipidome profile of patients responsive to anti-PD-1 treatment [26]. Furthermore, it is known that aromatase inhibitors alter the content of MUFA and PUFA in placental cells [14]. Our complex phospholipidome analysis indicated indeed that letrozole increased the MUFA + PUFA/SFA ratio. Letrozole responder cells had basally high levels of activated SREBP1c and target genes involved in FA synthesis (*ACLY*, *FASN*) and desaturation (*SCD1*). This endogenous apparatus makes letrozole responder cells more aggressive, since high levels of FASN [27] and SCD1 [28] have been associated to faster NSCLC progression. Letrozole, that further up-regulated FASN and SCD1, may potentially have deleterious effects. However, the net balance of this simultaneous activation of FASN and SCD1 was an increased PUFA + MUFA/SFA ratio. This occurs since PUFAs have a half-life of few hours [29], while SFAs have a shorter half-life because of their multiple metabolic fates, including FA oxidation or desaturation if SCD1 is up-regulated [30]. Mechanistically, the lipogenic process induced by letrozole, was caused by the increase in the intracellular content of testosterone that promoted the cleavage of SREBP1c into its active form, and resulted in higher content of LC-MUFAs and LC-PUFAs.

PD-L1 is an integral membrane protein and the interaction with more fluid (MUFA/PUFA-containing) PLs instead of more rigid (SFA-containing) PLs may affect its conformation, altering the efficient binding with PD-1. For instance, PD-L1 dimerization, favored by the lateral shift of PD-L1 molecules in a fluid plasma membrane, promotes its degradation, consequently reducing the binding to PD-1 [31].

Our results suggest that letrozole generates a MUFA/PUFA-rich lipid micro-environment that impairs the binding of PD-L1 to PD-1, in line with what observed in murine colon, urothelial and lung cancers where a high content of LC-PUFAs is associated with good response to anti-PD-1 treatment [18]. The proof of concept that membrane fluidity is the determinant factor in altering the PD-L1/PD-1 binding derived by the experimental setting with PA or DHA supplementation, that decreased and increased membrane fluidity, increased and decreased PD-L1/PD-1 binding, respectively. Interestingly, FASN inhibition, which was recently reported to increase the efficacy of anti-PD-1/PD-1L treatments in preclinical models of liver cancer [22], produced the same shift caused by letrozole in plasma membrane lipidome. Indeed, the FASN inhibitor Orlistat decreased the amount of PA, a typical SFA, but it produced only minor changes in DHA, a typical PUFA. This result is expected because the final product of FASN is PA, while DHA, as well as many other PUFAs, derive from the essential FAs linoleic acid and α-linolenic acid, and/or from multiple steps of intracellular desaturases and elongases that are independent from FASN [32].

The in vitro observations were confirmed in immune-xenografts, where DHA enhanced the efficacy of pembrolizumab in terms of reduced tumor growth and prolonged survival. The effects of DHA on plasma membrane fluidity, PD-L1/PD-1 binding and pembrolizumab efficacy were dose-dependent, but that high DHA dosage, well tolerated by the mice, abrogated the differences in sensitivity to pembrolizumab independently from their plasma membrane lipidome composition at baseline. The lower tumor growth can be attributed to the enhanced anti-tumor activity of TILs and to the higher attitude of PUFA-enriched cells to undergo immunogenic cell death [33]. Moreover, DHA has been reported to promote PD-L1 ubiquitination in NSCLC cells [34], in line with our results showing a decreased expression of PD-L1 in DHA-treated NSCLC xenografts. The sum of decreased membrane fluidity and PD-L1/PD-1 binding, increased immuno-activation and reduced PD-L1 level explains the antitumor efficacy of the combination pembrolizumab + DHA.

This work, demonstrating that the PUFA enrichment of plasma membrane PLs increased NSCLC sensitivity to anti-PD-1/anti-PD-L1 immunotherapy, may have important translational perspectives. Firstly, we suggest repurposing letrozole, an anti-tumor agent used in estrogen-dependent breast cancers, as a potential immuno-adjuvant agent in NSCLC, a tumor that is not considered hormone-dependent. Secondly, we highlight that the same benefit is produced by DHA, an orally available and well-tolerated ω3-FA integrator used in patients with cardiovascular diseases [35].

While there are not active trials evaluating the efficacy of aromatase inhibitors associated with ICIs in NSCLC, the first trial studying the impact of the dietary supplementation of ω3-FAs on immunotherapy response in NSCLC and on membrane phospholipid composition, has just started [NCT04965129] (www.trial.gov). Our data provide a strong mechanistic basis for the use of aromatase inhibitors and ω3-FAs in clinical settings, as potentially adjuvant agents for NSCLC patients non-responder to ICIs.

Funding

This work was supported by the Italian Association for Cancer Research (AIRC; IG21480 and IG29250 to CR); Fondazione Cassa di Risparmio di Torino (ID 2018.0568 and ID 2021.05556 to CR); Guido Berlucchi Foundation (Mini-Grant KOPJ_RIC_COMP_24_01 to JK), Italian Ministry of University and Research (PNRR - PNC - D3 4 HEALTH to ICS).

CRediT authors statement

Sofia La Vecchia performed the investigation in vitro, analyzed the data and wrote the original draft; Simona Fontana developed the methods on lipidome analysis; Iris Chiara Salaroglio and Dario Pasquale Anobile performed the in vivo experiments; Sabrina Digiovanni performed the flow cytometry experiments; Niloufar Jafari and Martina Godel performed the initial screening and analyzed the data; Muhlis Akman analyzed the lipidomic data; Costanzo Costamagna provided technical assistance in all the in vitro experiments; Cyril Corbet analyzed the data, reviewed and edited the final version; Joanna Kopecka and Chiara Riganti conceptualized the study, supervised the work, provided the funding, reviewed and edited the final version.

CRediT authorship contribution statement

Sofia La Vecchia: Writing – original draft, Investigation, Formal

analysis. **Simona Fontana:** Investigation, Formal analysis. **Iris Chiara Salaroglio:** Investigation, Formal analysis. **Dario Pasquale Anobile:** Investigation, Formal analysis. **Sabrina Digiovanni:** Investigation. **Muhlis Akman:** Methodology, Formal analysis. **Niloufar Jafari:** Investigation. **Martina Godel:** Investigation. **Costanzo Costamagna:** Methodology. **Cyril Corbet:** Writing – review & editing, Data curation. **Joanna Kopecka:** Writing – review & editing, Supervision, Resources, Conceptualization. **Chiara Riganti:** Writing – review & editing, Supervision, Resources, Conceptualization.

Declaration of competing interest

The authors declare that they have no known competing financial interests or personal relationships that could have appeared to influence the work reported in this paper.

Appendix A. Supplementary data

Supplementary data to this article can be found online at https://doi.org/10.1016/j.canlet.2024.217221.

References

[1] R.L. Siegel, K.D. Miller, H.E. Fuchs, A. Jemal, Cancer statistics, 2022, CA A Cancer J. Clin. 72 (1) (2022) 7–33, https://doi.org/10.3322/caac.21708.

[2] U. Dafni, Z. Tsourti, K. Vervita, S. Peters, Immune checkpoint inhibitors, alone or in combination with chemotherapy, as first-line treatment for advanced non-small cell lung cancer. A systematic review and network meta-analysis, Lung Cancer 134 (2019) 127–140, https://doi.org/10.1016/j.lungcan.2019.05.029.

[3] M. Tagliamento, P. Bironzo, H. Curcio, E. De Luca, D. Pignataro, S.G. Rapetti, M. Audisio, V. Bertaglia, C. Paratore, M. Bungaro, E. Olmetto, E. Artusio, M. L. Reale, C. Zichi, E. Capelletto, S. Carnio, L. Buffoni, F. Passiglia, S. Novello, G. V. Scagliotti, M. Di Maio, A systematic review and meta-analysis of trials assessing PD-1/PD-L1 immune checkpoint inhibitors activity in pre-treated advanced stage malignant mesothelioma, Crit. Rev. Oncol. Hematol. 172 (2022) 103639, https://doi.org/10.1016/j.critrevonc.2022.103639.

[4] C.J.D. Wallis, M. Butaney, R. Satkunasivam, S.J. Freedland, S.P. Patel, O. Hamid O, S.K. Pal, Z. Klaassen, Association of patient sex with efficacy of immune checkpoint inhibitors and overall survival in advanced cancers: a systematic review and meta-analysis, JAMA Oncol. 5 (4) (2019) 529–536, https://doi.org/10.1001/jamaoncol.2018.5904.

[5] C. Wang, W. Qiao, Y. Jiang, M. Zhu, J. Shao, P. Ren, D. Liu, W. Li, Effect of sex on the efficacy of patients receiving immune checkpoint inhibitors in advanced non-small cell lung cancer, Cancer Med. 8 (8) (2019) 4023–4031, https://doi.org/10.1002/cam4.2280.

[6] T. Vavalà, A. Catino, P. Pizzutilo, V. Longo, D. Galetta, Gender differences and immunotherapy outcome in advanced lung cancer, Int. J. Mol. Sci. 22 (21) (2021) 11942, https://doi.org/10.3390/ijms222111942.

[7] L.P. Stabile, A.L. Davis, C.T. Gubish, T.M. Hopkins, J.D. Luketich, N. Christie, S. Finkelstein, J.M. Siegfried, Human non-small cell lung tumors and cells derived from normal lung express both estrogen receptor alpha and beta and show biological responses to estrogen, Cancer Res. 62 (7) (2002) 2141–2150.

[8] T. Smida, T.C. Bruno, L.P. Stabile, Influence of estrogen on the NSCLC microenvironment: a comprehensive picture and clinical implications, Front. Oncol. 10 (2020) 137, https://doi.org/10.3389/fonc.2020.00137.

[9] X.Z. Zhao, Y. Liu, L.J. Zhou, Z.Q. Wang, Z.H. Wu, X.Y. Yang, Role of estrogen in lung cancer based on the estrogen receptor-epithelial mesenchymal transduction signaling pathways, OncoTargets Ther. 8 (2015) 2849–2863, https://doi.org/10.2147/OTT.S90085.

[10] M. Grott, S. Karakaya, F. Mayer, F. Baertling, C. Beyer, M. Kipp M, H.G. Kopp, Progesterone and estrogen prevent cisplatin-induced apoptosis of lung cancer cells, Anticancer Res. 33 (2013) 791–800.

[11] Z. Wang, Z. Li, X. Ding, Z. Shen, Z. Liu, T. An, J. Duan, J. Zhong, M. Wu, J. Zhao, M. Zhuo, Y. Wang, S. Wang, Y. Sun, H. Bai, J. Wang, ERβ localization influenced outcomes of EGFR-TKI treatment in NSCLC patients with EGFR mutations, Sci. Rep. 5 (2015) 11392, https://doi.org/10.1038/srep11392.

[12] M.A. Velez, T.F. Burns, L.P. Stabile, The estrogen pathway as a modulator of response to immunotherapy, Immunotherapy 11 (13) (2019) 1161–1176, https://doi.org/10.2217/imt-2019-0024.

[13] D.P. Anobile, I.C. Salaroglio, F. Tabbò, S. La Vecchia, M. Akman, F. Napoli, M. Bungaro, F. Benso, E. Aldieri, P. Bironzo, J. Kopecka, F. Passiglia, L. Righi, S. Novello, G.V. Scagliotti, C. Riganti, Autocrine 17-β-Estradiol/Estrogen receptor-α loop determines the response to immune checkpoint inhibitors in non-small cell lung cancer, Clin. Cancer Res. 29 (19) (2023) 3958–3973, https://doi.org/10.1158/1078-0432.CCR-22-3949.

[14] E. Pérez-Albaladejo, S. Lacorte, C. Porte, Differential toxicity of alkylphenols in JEG-3 human placental cells: alteration of P450 aromatase and cell lipid composition, Toxicol. Sci. 167 (2) (2019) 336–346, https://doi.org/10.1093/toxsci/kfy243.

[15] M.E. King, R. Yuan, J. Chen, K. Pradhan, I. Sariol, S. Li, A. Chakraborty, O. Ekpenyong, J.H. Yearley, J.C. Wong, L. Zúñiga, D. Tomazela, M. Beaumont, J. H. Han, L.S. Eberlin, Long-chain polyunsaturated lipids associated with responsiveness to anti-PD-1 therapy are colocalized with immune infiltrates in the tumor microenvironment, J. Biol. Chem. 299 (3) (2023) 102902, https://doi.org/10.1016/j.jbc.2023.102902.

[16] L.D. Shultz, B.L. Lyons, L.M. Burzenski, B. Gott, X. Chen, S. Chaleff, M. Kotb, S. D. Gillies, M. King, J. Mangada, D.L. Greiner, R. Handgretinger, Human lymphoid and myeloid cell development in NOD/LtSz-scid IL2R gamma null mice engrafted with mobilized human hemopoietic stem cells, J. Immunol. 174 (10) (2005) 6477–6489, https://doi.org/10.4049/jimmunol.174.10.6477.

[17] A.M. Coughlan, C. Harmon, S. Whelan, E.C. O'Brien, V.P. O'Reilly, P. Crotty, P. Kelly, M. Ryan, F.B. Hickey, C. O'Farrelly, M.A. Little, Myeloid engraftment in humanized mice: impact of granulocyte-colony stimulating factor treatment and transgenic mouse strain, Stem Cell. Dev. 25 (7) (2016) 530–541, https://doi.org/10.1089/scd.2015.0289.

[18] M. Zhao, H. Yuan, G. Yang, Y. Wang, Y. Bu, H. Zhang, L. Zhao, P. Lv, H. Yun, Y. Geng, J. Feng, C. Hou, S. Wang, N. Zhang, W. Lu, X. Zhang, Tumour cell-expressed PD-L1 reprograms lipid metabolism via EGFR/ITGB4/SREBP1c signalling in liver cancer, JHEP Rep 6 (4) (2024) 101009, https://doi.org/10.1016/j.jhepr.2024.101009.

[19] F. Zhang, T. Pan, L.D. Nielsen, R.J. Mason, Lipogenesis in fetal rat lung: importance of C/EBPalpha, SREBP-1c, and stearoyl-CoA desaturase, Am. J. Respir. Cell Mol. Biol. 30 (2) (2004) 174–183, https://doi.org/10.1165/rcmb.2003-0235OC.

[20] H. Heemers, B. Maes, F. Foufelle, W. Heyns, G. Verhoeven, J.V. Swinnen, Androgens stimulate lipogenic gene expression in prostate cancer cells by activation of the sterol regulatory element-binding protein cleavage activating protein/sterol regulatory element-binding protein pathway, Mol. Endocrinol. 15 (10) (2001) 1817–1828, https://doi.org/10.1210/mend.15.10.0703.

[21] A.M. Gouw, L.S. Eberlin, K. Margulis, D.K. Sullivan, G.G. Toal, L. Tong, R.N. Zare, D.W. Felsher, Oncogene KRAS activates fatty acid synthase, resulting in specific ERK and lipid signatures associated with lung adenocarcinoma, Proc. Natl. Acad. Sci. U.S.A. 114 (17) (2017) 4300–4305, https://doi.org/10.1073/pnas.1617709114.

[22] J. Huang, W.Y. Tsang, X.N. Fang, Y. Zhang, J. Luo, L.Q. Gong, B.F. Zhang, C. N. Wong, Z.H. Li, B.L. Liu, J.L. Huang, Y.M. Yang, S. Liu, L.X. Ban, Y.H. Chan, X. Y. Guan, FASN inhibition decreases MHC-I degradation and synergizes with PD-L1 checkpoint blockade in hepatocellular carcinoma, Cancer Res. 84 (6) (2024) 855–871, https://doi.org/10.1158/0008-5472.CAN-23-0966.

[23] M. Sankaranarayanapillai, N. Zhang, K.A. Baggerly, J.G. Gelovani, Metabolic shifts induced by fatty acid synthase inhibitor orlistat in non-small cell lung carcinoma cells provide novel pharmacodynamic biomarkers for positron emission tomography and magnetic resonance spectroscopy, Mol. Imag. Biol. 15 (2) (2013) 136–147, https://doi.org/10.1007/s11307-012-0587-6.

[24] G. Lei, L. Zhuang, B. Gan, Targeting ferroptosis as a vulnerability in cancer, Nat. Rev. Cancer 22 (7) (2022) 381–396, https://doi.org/10.1038/s41568-022-00459-0.

[25] L. Liu, M. Mo, X. Chen, D. Chao, Y. Zhang, X. Chen, Y. Wang, N. Zhang, N. He, X. Yuan, H. Chen, J. Yang, Targeting inhibition of prognosis-related lipid metabolism genes including CYP19A1 enhances immunotherapeutic response in colon cancer, J. Exp. Clin. Cancer Res. 42 (1) (2023) 85, https://doi.org/10.1186/s13046-023-02647-8.

[26] L. Liu, S. Zhang, H.Y. Yang, C.H. Zhou, Y. Xiong, N. Yang, Y. Tian, Lipid alterations play a role in the integration of PD-1/PD-L1 inhibitors and anlotinib for the treatment of advanced non-small-cell lung cancer, Lipids Health Dis. 23 (1) (2024) 16, https://doi.org/10.1186/s12944-023-01960-7.

[27] Y. Chen, Y. Zhou, R. Ren, Y. Chen, J. Lei, Y. Li, Harnessing lipid metabolism modulation for improved immunotherapy outcomes in lung adenocarcinoma, J. Immunother Cancer 12 (7) (2024) e008811, https://doi.org/10.1136/jitc-2024-008811.

[28] J. Zhang, F. Song, X. Zhao, H. Jiang, X. Wu, B. Wang, M. Zhou, M. Tian, B. Shi, H. Wang, Y. Jia, H. Wang, X. Pan, Z. Li, EGFR modulates monounsaturated fatty acid synthesis through phosphorylation of SCD1 in lung cancer, Mol. Cancer 16 (1) (2017) 127, https://doi.org/10.1186/s12943-017-0704-x.

[29] S.I. Rapoport, Translational studies on regulation of brain docosahexaenoic acid (DHA) metabolism in vivo, Prostaglandins Leukot. Essent. Fatty Acids 88 (1) (2013) 79–85, https://doi.org/10.1016/j.plefa.2012.05.003.

[30] G. Carta, E. Murru, S. Banni, C. Manca, Palmitic acid: physiological role, metabolism and nutritional implications, Front. Physiol. 8 (2017) 902, https://doi.org/10.3389/fphys.2017.00902.

[31] X. Wu, N. Wang, J. Liang, B. Wang, Y. Jin, B. Liu, Y. Yang, Is the triggering of PD-L1 dimerization a potential mechanism for food-derived small molecules in cancer immunotherapy? A study by molecular dynamics, Int. J. Mol. Sci. 24 (2) (2023) 1413, https://doi.org/10.3390/ijms24021413.

[32] A.F. Domenichiello, A.P. Kitson, R.P. Bazinet, Is docosahexaenoic acid synthesis from α-linolenic acid sufficient to supply the adult brain? Prog. Lipid Res. 59 (2015) 54–66, https://doi.org/10.1016/j.plipres.2015.04.002.

[33] G. Gelsomino, P.A. Corsetto, I. Campia, G. Montorfano, J. Kopecka, B. Castella, E. Gazzano, D. Ghigo, A.M. Rizzo, C. Riganti, Omega 3 fatty acids chemosensitize multidrug resistant colon cancer cells by down-regulating cholesterol synthesis and

altering detergent resistant membranes composition, Mol. Cancer 12 (2013) 137, https://doi.org/10.1186/1476-4598-12-137.
[34] H. Zhang, H. Chen, S. Yin, L. Fan, C. Jin, C. Zhao, H. Hu, Docosahexaenoic acid reverses PD-L1-mediated immune suppression by accelerating its ubiquitin-proteasome degradation, J. Nutr. Biochem. 112 (2023) 109186, https://doi.org/10.3390/10.1016/j.jnutbio.2022.109186.
[35] E.J. Baker, Alternative sources of bioactive omega-3 fatty acids: what are the options? Curr. Opin. Clin. Nutr. Metab. Care 27 (2) (2024) 106–115, https://doi.org/10.1097/MCO.0000000000001006.

Supplementary Materials

Supplementary Table S1. Features of the non-small cell lung cancer cell lines

Cell line	ATCC number	Gender	Age	Smoke	Site	Histotype
A549	CRM-CCL-185	M	58	n.d.	P	Adeno
NCI-H1385	CRL-5867	F	49	Y	M	Adeno
NCI-H1435	CRL-5870	F	35	N	P	Adeno
NCI-H1734	CRL-5891	F	56	N	P	Adeno
NCI-H1793	CRL-5896	F	52	N	P	Adeno
NCI-H2347	CRL-5942	F	54	N	P	Adeno
NCI-H2073	CRL-5918	F	47	Y	P	Adeno
NCI-H2228	CRL-5935	F	n.d.	N	P	Adeno
NCI-H2066	CRL-5868	F	70	n.d.	P	Mixed (adeno-squaamous)
NCI-H2286	CRL-5938	F	57	Y	P	Mixed (adeno-squamous)
Calu-3	HTB-55	M	25	n.d.	P	Adeno
NCI-H2087	CRL-5922	M	69	Y	M	Adeno
NCI-H23	CRL-5800	M	51	n.d.	P	Adeno
NCI-H2126	CCL-256	M	65	n.d.	M	Adeno
NCI-H1299	CRL-5803	M	43	n.d.	M	Adeno
NCI-H1437	CRL-5872	M	60	Y	M	Adeno
NCI-H1563	CRL-5875	M	n.d.	N	P	Adeno
NCI-H661	HTB-183	M	43	n.d.	M	Adeno
NCI-H522	CRL-5810	M	58	Y	P	Adeno

NCI-H1651	CRL-5884	M	71	N	P	Adeno
NCI-H2085	CRL-5921	M	45	n.d.	n.d.	Adeno
NCI-H2342	CRL-5941	M	55	N	P	Adeno
NCI-H1703	CRL-5889	M	54	Y	P	Squamous
NCI-H441	CRM-HTB-174	M	n.d.	n.d.	M	Adeno
NCI-H596	HTB-178	M	73	n.d.	P	Mixed (adeno-squamous)
NCI-H2170	CRL-5928	M	n.d.	N	P	Squamous
NCI-H460	HTB-177	M	n.d.	n.d.	M	Adeno
NCI-H1650	CRL-5883	M	27	Y	P	Adeno
NCI-H1975	CRL-5908	F	n.d.	N	P	Adeno

F: female; M: male; Y: yes; N: no; P: primary tumor; M: metastasis; n.d.: not determined; Adeno: adenocarcinoma.

Supplementary Table S2. Lipidome profile in poor and good responders non-small cell lung cancer cells

Mean scaled intensity of lipid types in letrozole-treated cells versus the untreated cells (n = 5 independent experiments) and statistical analysis. Bold numbers: statistically significant results.

See Excel file

Supplementary Table S3. Primers list for qRT-PCR

Gene	Forward primer	Reverse primer
ACLY	GCTCTGCCTATGACAGCACCAT	GTCCGATGATGGTCACTCCCTT
ACC	GAATTTGTCACCCGCTTTGG	TGGAGCGCATCCACTTGA
FASN	TTCTACGGCTCCACGCTCTTCC	GAAGAGTCTTCGTCAGCCAGGA
SCD1	CCTGGTTTCACTTGGAGCTGTG	TGTGGTGAAGTTGATGTGCCAGC
SCD2	CAGCGTGCCTCCTCTCCTAAT	TGTGTTGCCATATTTTAGTGTCACA
SREBP1	ACTTCTGGAGGCATCGCAAGCA	AGGTTCCAGAGGAGGCTACAAG
S14	GGTGCAAGGAGCTGGGTAT	TCCAGGGGTCTTGGTCCTATTT

ACLY: ATP citrate lyase; *ACC*: acetyl-CoA carboxylase; *FASN*: fatty acid synthase; *SCD1*: stearoyl-CoA desaturase 1; *SCD2*: stearoyl-CoA desaturase 2; *SREBP1*: sterol regulatory element binding protein 1.

Supplementary Table S4. Immunophenotype of the circulating immune cells detected in the cohorts of Hu-CD34$^+$ mice used in the study

			Lymphoid cells	Myeloid cells		
Cohort	Weight	hCD45$^+$	hCD19$^+$	hCD3$^+$	hCD33$^+$	mCD45$^+$
(donor)	(g)	(% total)	(% of hCD45$^+$)	(% of hCD45$^+$)	(% of hCD45$^+$)	(% total)
#1	24.6 ± 2.5	65.8 ± 5.9	69.1 ± 7.4	19.3 ± 3.8	7.1 ± 2.5	34.2 ± 6.8
#2	25.9 ± 1.6	73.0 ± 6.8	66.8 ± 6.3	21.0 ± 2.6	7.5 ± 2.9	27.0 ± 3.4
#3	27.0 ± 2.3	74.6 ± 7.2	66.3 ± 5.6	24.0 ± 4.5	8.9 ± 2.5	25.4 ± 6.1
#4	26.2 ± 2.1	61.5 ± 6.3	62.3 ± 8.1	29.1 ± 4.9	5.5 ± 2.1	38.5 ± 6.7
#5	23.2 ± 3.4	67.5 ±6.2	69.1 ± 8.9	21.8 ± 4.5	9.3 ± 2.1	32.6 ± 4.4
#6	25.5 ± 3.2	63.9 ± 8.2	67.0 ± 6.3	23.0 ± 2.4	8.8 ± 3.4	36.1 ± 7.8
#7	25.2 ± 2.7	67.5 ± 6.7	62.9 ± 5.3	26.8 ± 3.6	9.7 ± 2.1	32.5 ± 4.1
#8	26.8 ± 1.9	65.4 ± 6.3	70.1 ± 5.7	25.7 ± 4.5	6.9 ± 3.4	34.6 ± 4.9

Data are mean ± SD of weight and immune cell populations in each cohort of mice used in the study, where one cohort is composed by mice engrafted with cells from the same human donor. H: human; m: murine.

Supplementary Figures

Figure S1

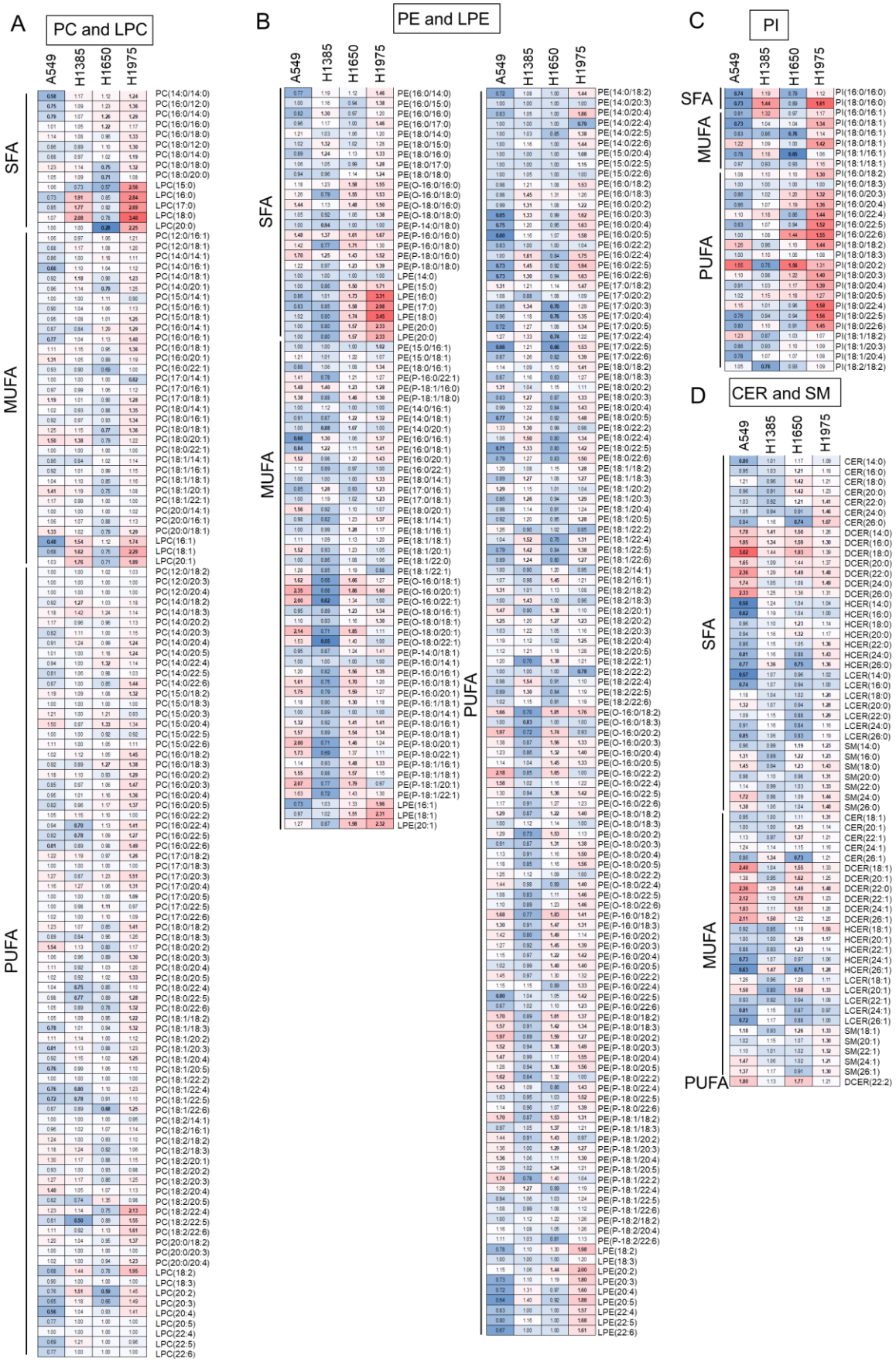

Supplementary Figure S1. Phospholipid abundance in NSCLC cells. Cells were treated with or without the letrozole 10 nM for 24 h, then used for lipidomic analyses of phospholipids. Untreated cells were grown in fresh medium containing 0.1% v/v DMSO. Heatmaps of phosphatidylcholines (PC) and lysophosphatidylcholines (LPC) (**A**), phosphatidylethanolamines (PE) and lysophosphatidylethanolamines (LPE) (**B**), phosphoinositides (PI) (**C**), ceramides (CER) and sphingomyelines (SM) (**D**). SFA: saturated fatty acids; MUFA: monounsaturated fatty acids; PUFA: polyunsaturated fatty acids. Data are mean scaled intensity for a metabolite in letrozole-treated cells versus untreated cells (n = 5 independent experiments). Red: upregulated lipids; blue: downregulated lipids; bold: statistically significant results.

Figure S2

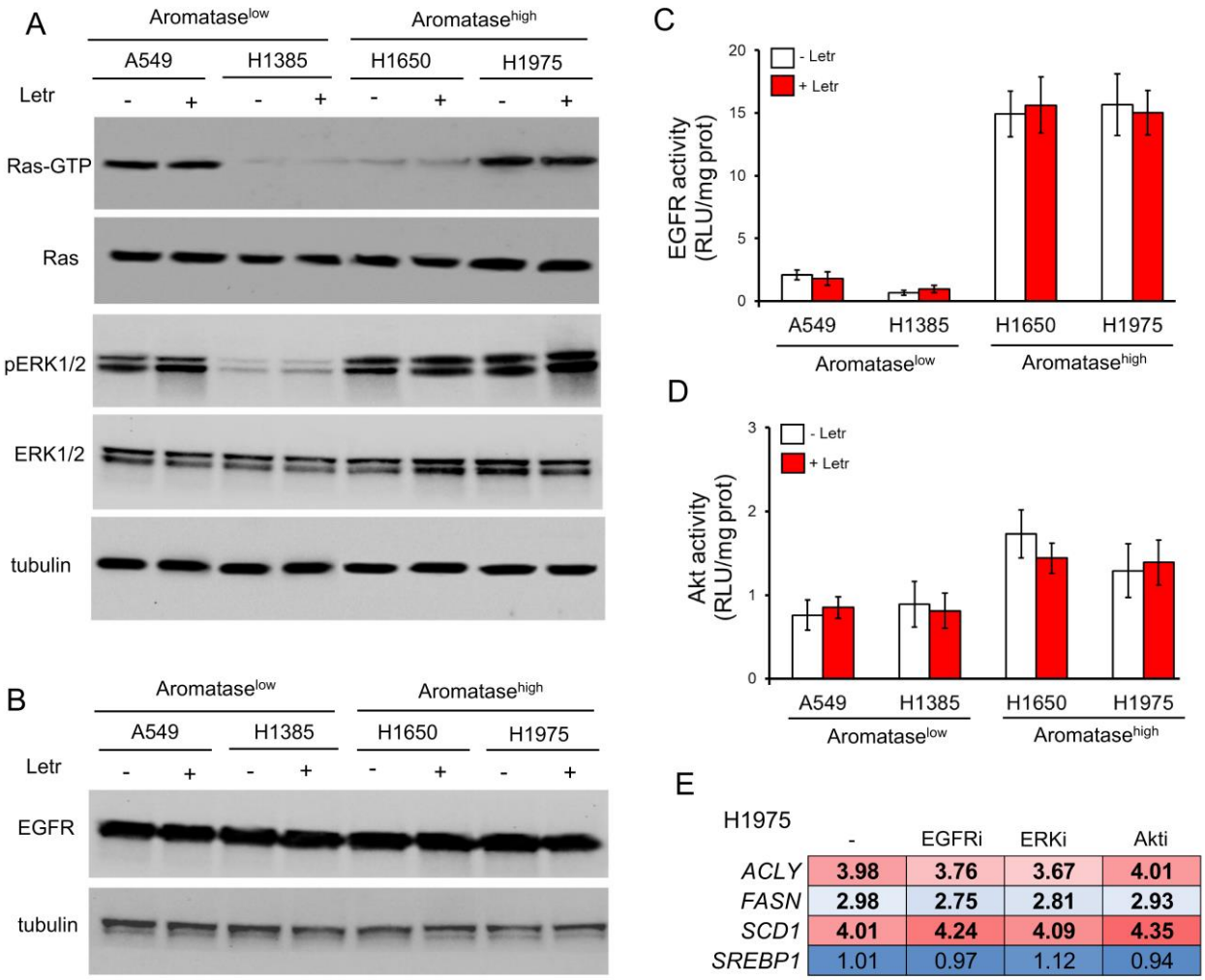

E

H1975

	-	EGFRi	ERKi	Akti
ACLY	**3.98**	**3.76**	**3.67**	**4.01**
FASN	**2.98**	**2.75**	**2.81**	**2.93**
SCD1	**4.01**	**4.24**	**4.09**	**4.35**
SREBP1	1.01	0.97	1.12	0.94

Supplementary Figure S2. **Effects of Ras/ERK and EGFR/Akt axes on SREBP1c activity in NSCLC cells.** Cells were treated with (+) or without (-) the letrozole (Letr;10 nM). "- Letr" cells: cells grown in fresh medium containing 0.1% v/v DMSO. (**A**) Pull-down of Ras-GTP, considered an index of active Ras, and immunoblot of total Ras, phospho(Thr202/Tyr204)ERK1/2, total ERK1/2. Tubulin has been used as a control of equal protein levels. The image is representative of 1 out of 3 experiments. (**B**) Immunoblotting of EGFR in cell lysates. Tubulin has been used as a control of equal protein levels. The image is representative of 1 out of 3 experiments. (**C-D**) EGFR and Akt activity, measured by chemiluminescence-based assays. Data are shown as the mean ± SD (n = 3 independent experiments, in technical duplicates). (**E**) NCI-H1975 cells were grown 24 h in fresh medium (-), in medium containing the EGFR inhibitor AZD9291 (1 µM, EGFRi), the ERK1/2 inhibitor U-0126 (10 µM, ERKi) or the Akt inhibitor MK-2206 (1 µM, Akti). Heatmap of lipogenic genes, measured by qRT-PCR. Data are the mean of normalized gene expression in letrozole-treated cells versus untreated cells (n = 3 independent experiments, in technical triplicates). Red: upregulated genes; blue: downregulated genes; bold: statistically significant results.

Figure S3

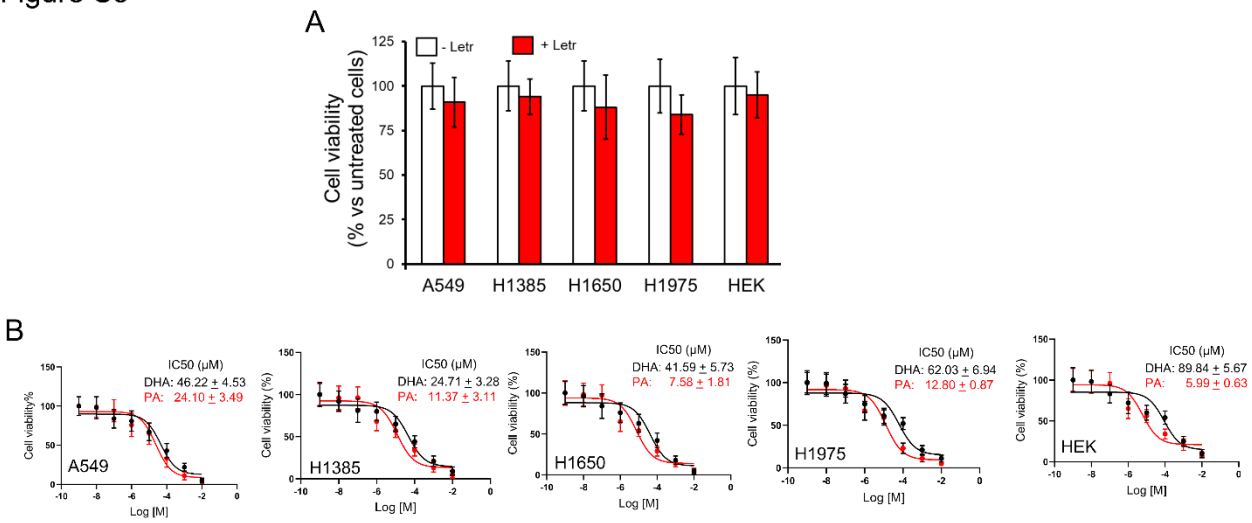

Supplementary Figure S3. Viability of NSCLC cells treated with letrozole, palmitic acid and docosahexaenoic acid. (A) Cells were treated with (+) or without (-) the letrozole (Letr;10 nM) for 24h, then the viability was measured spectrophotometrically. "- Letr" cells: cells grown in fresh medium containing 0.1% v/v DMSO. Cell viability was expressed as percentage of treated versus untreated cells taken as 100% viability. Data are shown as the mean ± SD (n = 3 independent experiments, in technical quadruplicates). (**B**) Cells were incubated for 24 h with increasing concentrations (from 10^{-10} to 10^{-2} M) of palmitic acid (PA) or docosahexaenoic acid (DHA). Untreated were grown in fresh medium containing BSA-ethanol 0.1% v/v. Data are shown as the mean ± SEM (n = 3, in technical quadruplicates). The IC50 was calculated with the GraphPad software.

Figure S4

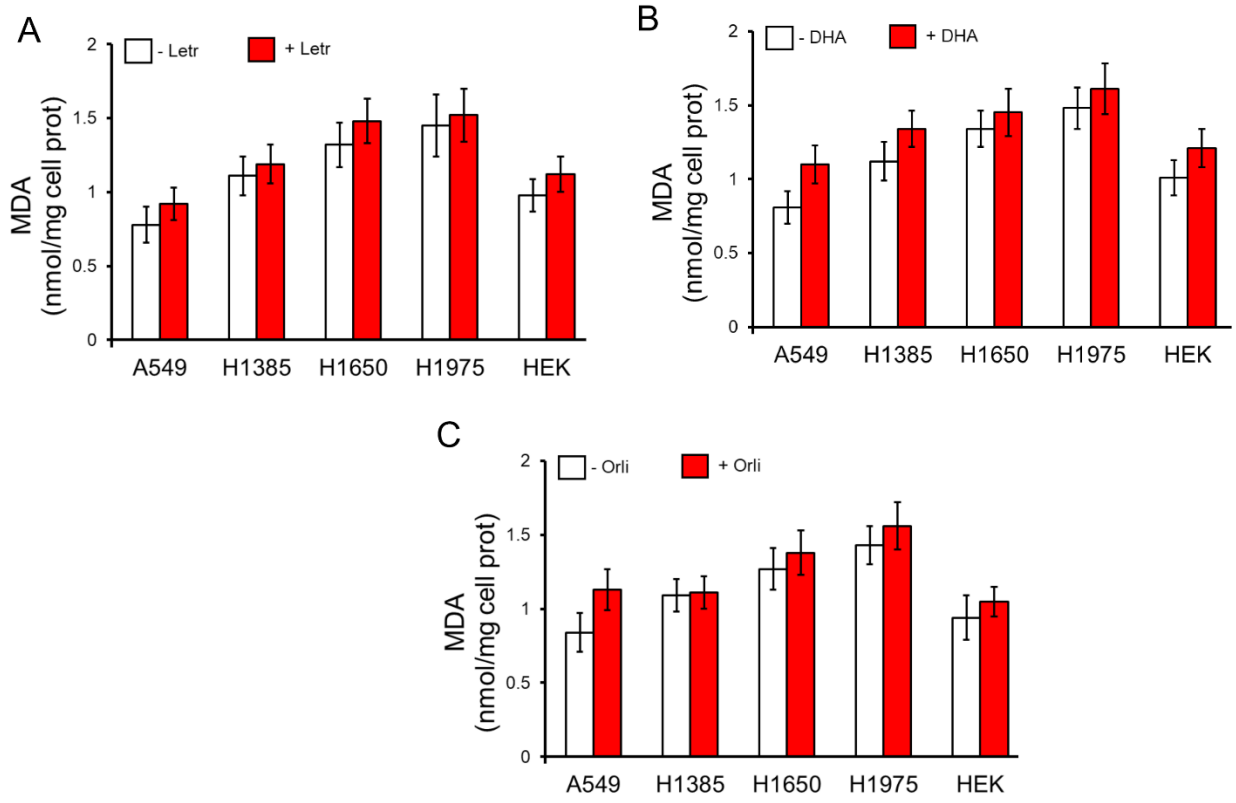

Supplementary Figure S4. Effects of letrozole, docosahexaenoic acid and Orlistat on lipid peroxidation. Cells were treated 24 h with fresh medium containing DMSO 0.1% (ctrl) or letrozole (Letr;10 nM, **A**), docosahexaenoic acid (DHA at the IC50 of each cell line, calculated in Fig. S3B; **B)** or Orlistat (Orli; 30 µM, **C**). Malonyl dialdehyde (MDA) levels, considered an index of lipid peroxidation, were measured fluorimetrically. Data are shown as the mean ± SD (n = 3 independent experiments, in technical duplicates).

Figure S5

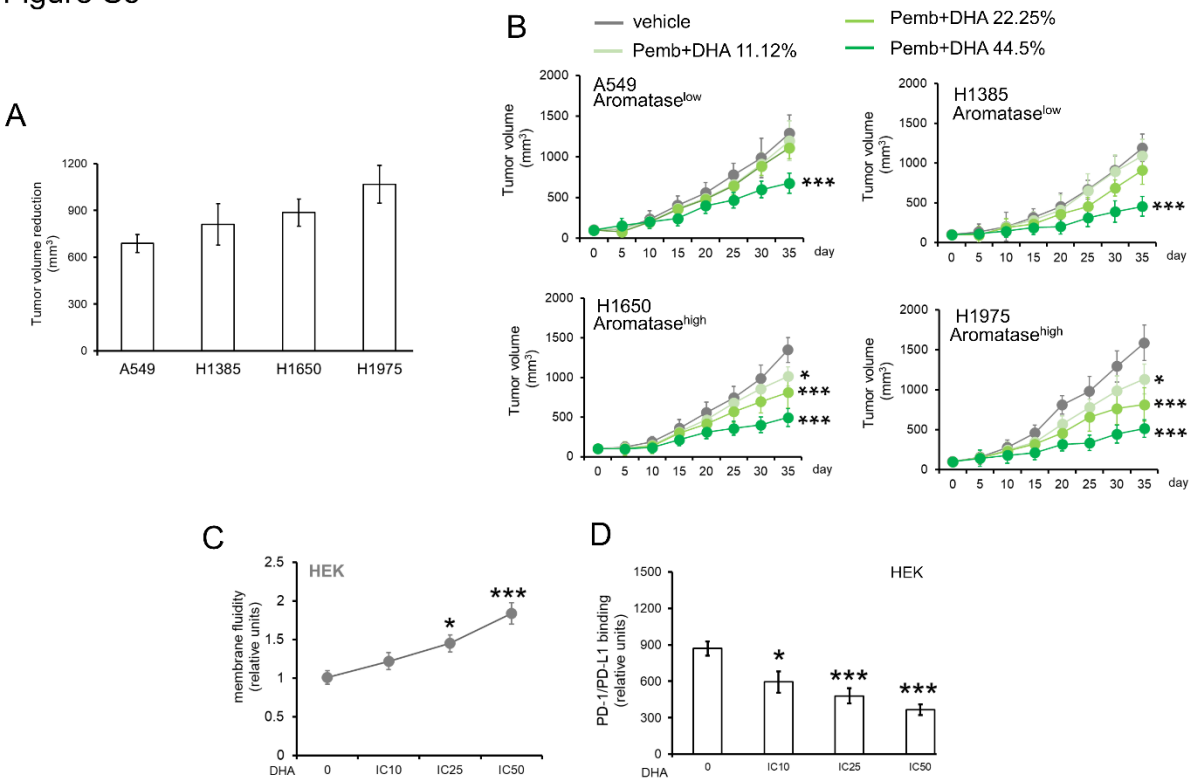

Supplementary Figure S5. Dose-dependent effects of docosahexaenoic acid. (**A**) Hu-CD34^{+} mice were injected subcutaneously with human 1×10^{6} NSCLC cells (A549, H1385, H1650, H1975), mixed with 100 µl Matrigel. When tumor volume reached 100 mm^{3}, mice were randomized and treated with: vehicle (saline solution), pembrolizumab (Pemb), DHA or their combination (Pemb+DHA) for 35 days as in Figure 4. Difference between tumor volume in vehicle-treated group and tumor volume in pembrolizumab+DHA-treated group at day 40. Data are the mean ± SD (n = 10 mice/group). **(B)** Mice (n=4/group) were treated with vehicle (saline solution), Pemb+DHA 11.12% v/v, Pemb+DHA 22.25% v/v, Pemb+DHA 44.5% v/v. Tumor growth was monitored by a caliper and animals were euthanized at day 40. Data are shown as the mean ± SD (n = 4 mice/group). *p<0.05, ***p<0.001: treated groups vs vehicle group. (**C**) Membrane fluidity, measured fluorometrically in HEK293 cells, grown for 24 h without (0) or with docosahexaenoic acid (DHA) at IC510, IC25 or IC50 (calculated in Fig. S3B). Data are shown as the mean ± SD (n = 3 independent experiments, in technical duplicates). *p<0.05, ***p<0.001: DHA-treated vs untreated cells. (**D**) PD-L1/PD-1 binding assay, measured in HEK293 cells incubated as described in (**C**). Data are shown as the mean ± SD (n = 3 independent experiments). *p<0.05, ***p<0.001: DHA-treated treated vs untreated cells.